Received 15 December 2025, accepted 27 May 2026, date of publication 30 June 2026
www.computingonline.net / computing@computingonline.net

Print ISSN 1727-6209
Online ISSN 2312-5381
DOI 10.47839/ijc.25.2.4649

A Novel EBOwithCMAR Hybrid Algorithm for Single and Multi-Objective Optimal Power Flow

İBRAHIM ÇAGRI BARUTÇU[1], VOLKAN YAMAÇLI[2], HAKAN IŞIKER[3], KADIR ABACI[3], ELİF ECE ELMAS[4]

[1]Department of Electricity and Energy, Çölemerik V.H.S., Hakkari University, P. O. Box 30000, Hakkari, Türkiye
[2]Department of Computer Engineering, Faculty of Engineering, Mersin University, P. O. Box 33343, Mersin, Türkiye
[3]Department of Electrical and Electronics Engineering, Faculty of Engineering, Mersin University, P. O. Box 33343, Mersin, Türkiye
[4]Department of Military Electronic Systems Engineering, Alparslan Defence Sciences and National Security Institute, National Defence University, 06654, Ankara, Türkiye

Corresponding author: Elif Ece ELMAS (e-mail: elifece.elmas@msu.edu.tr)

ABSTRACT In this paper, we present a solution for both single-objective optimal power flow (SOOPF) and multi-objective optimal power flow (MOOPF) problems using the EBOwithCMAR algorithm, which combines the Effective Butterfly Optimiser (EBO), Covariance Matrix Adapted Withdrawal Stage (CMAR) and Least Squares (LS) techniques, competing with the benchmark problems in CEC-2017 and the winning solutions of CEC-2016. The EBO applies a crossover operator that enhances population diversity during the Perching and Patrolling phases. CMAR allows for comprehensive optimization of solutions after identifying promising regions, while the LS method improves the precision and accuracy of the final solutions through a more targeted search. This study highlights the individual roles of each component within the EBOwithCMAR algorithm in the optimization process. We have successfully implemented the EBO, EBOCMAR, and EBOCMARLS (EBOwithCMAR) algorithms to address SOOPF and weighted method MOOPF problems in standard IEEE 30 test system, including those with renewable energy sources. The results are promising compared to well-established algorithms in the literature, all while maintaining compliance with system constraints.

KEYWORDS EBO, CMAR, EBOwithCMAR, Optimal Power Flow, Multi-objective Optimal Power Flow.

I. INTRODUCTION

The optimal power flow (OPF) is a complex problem characterized by its nonlinear, non-convex nature and large-scale dimensions. It involves optimizing various objective functions by determining the best settings for control variables while adhering to equality and inequality constraints [1]. Using sustainable energy, environmental concerns, economic factors, and the necessity for stable grid operation without compromising system operational and safety limits presents a complex challenge. Consequently, the Optimal Power Flow (OPF) problem has evolved into a multi-objective optimization problem [2]. Recently, there has been a growing interest in multi-objective optimal power flow (MO-OPF) studies that aim to simultaneously minimize multiple objective functions, addressing the intricate challenges faced by modern power systems. As a result, MO-OPF has become an essential tool for power system operators and planners, enabling the simultaneous evaluation of competing objectives such as cost reduction, emission control, power loss minimization, and system reliability.

Research on multi-objective evolutionary algorithms (MOEAs) and classical methods are the two most popular approaches for finding optimal multi-objective solutions to minimize multiple objective functions [3]. While multi-objective (MO) approaches produce a set of optimal solutions, known as the Pareto set, traditional optimization methods yield only a single solution point. By assigning appropriate weighting factors to each objective, conventional methods can reduce multi-objective problems to single-objective problems. The aim is to establish a correlation between the range of each objective function and its corresponding weight. For instance, an objective function with an extensive range should be given a smaller weight [4]. Decision-makers can determine suitable weights by following this relationship. The optimal weights are determined based on each objective function's maximum

range, which helps reduce the required computational effort [5].

A. LITERATURE REVIEW

The multi-objective optimization problem formulation (MOOPF) has been extensively researched over the past three decades, utilizing both classical and multi-objective evolutionary algorithms. Various meta-heuristic algorithms have been successfully implemented within both frameworks to address this problem. Many studies employ weight coefficients to relate the different objective functions to one another. In [6], the weighted sum method with the modified weighted teaching learning-based optimization (WTLBO) algorithm was used to convert multi-objective functions into a single objective function. The OPF problem is solved using the Artificial Bee Colony (ABC) method in [7], which considers equality and inequality restrictions in an electric power system. The non-convex single and multi-goals optimal power flow (OPF) problem is solved in [8] using the chaotic-quasi-oppositional-phasor based multi populations gorilla troop optimizer (MGTO). In [9], the single and multi-objective OPF problem is tackled using the chaotic equilibrium optimization (CEO) algorithm, which incorporates weights for the objective functions in the solution. [10] suggests a different method for handling the multi-objective OPF problem with the weight coefficient. The article presents the Improved Archimedes Optimization Algorithm (IAOA), compares it to other methods in the literature, and applies it to single and multi-objective goals. In [11], the effectiveness of the BSA method for solving different OPF problems with complicated and non-smooth objective functions has been proposed. In [12], researchers introduce and evaluates new variants of the Successive History-based Adaptive Differential Evolutionary (SHADE) algorithm called ESHADE, SHADE-SFS, and SHADE-SAP to solve the single and multi-objective OPF problems with equality and inequality constraints. A hybrid sine cosine-grey wolf optimizer (HSC-GWO) algorithm is proposed for solving a multi-objective (OPF) problem in a large real-time grid [13]. In [14], the OPF problem was solved for single and weighted sum multi-objective cases by combining constraint handling (CH) techniques and self-adaptive (SP) penalty functions and integrating them into the differential evolution (ECHT-DE) algorithm for IEEE 30, IEEE 57 and IEEE 118-bus systems.

In addition to these studies, improved moth flame optimization (IMFO) [15] uses the weight coefficient, the Differential Search Algorithm (DSA) [16], the Improved Colliding Bodies Optimization algorithm (ICBO) [17], and the Moth Swarm Algorithm (MSA) [18] are used to solve the MOOPF problem. These approaches are straightforward and can be employed for single-objective algorithms without modification. In literature, many studies present the weighting method for the multi-objective OPF problem and the multi-objective evolutionary program (MOEA) and suggest the optimum solution point to decision-makers by accurately describing the Pareto optimal front. In [19], researchers utilized the shuffle frog leaping algorithm (SFLA) to address the multi-objective OPF problem with a focus on emissions. To overcome the challenge of tuning control parameters, the authors of [20] proposed an enhanced self-adaptive DE and a mix crossover operator (ESDE-MC) capable of handling single and multi-objective OPF problems. A technique called the quasi-oppositional teaching learning-based optimization (QOTLBO) algorithm was introduced in [21], which involves integrating the quasi-oppositional learning algorithm into the teaching learning-based optimization (TLBO) algorithm to enhance convergence speed and solution quality. Furthermore, the authors of [22] recommended a modified TLBO (MTLBO) to address the MOOPF problem with emission and cost objectives. In [3], the multi-objective search group algorithm (MOSGA) is proposed as a new multi-objective method that efficiently solves the multi-objective optimal power flow (MOOPF) problem in power systems. Renewable energy sources have gained value recently due to their sustainability, abundance, and environmental friendliness. They have been increasingly appreciated in power systems, which has led to the implementation of various Pareto concept-based meta-heuristic techniques such as Memory-Guided JAYA (MG-JAYA) [23], MJAYA [24], NSGA-II [25], non-dominated sorting (NS) particle swarm optimization (SCNSPSO) [26], NDS Grey Wolf Optimizer [27], multi-objective mayfly algorithm (NSMA-SF) [28] to the MOOPF problem. In [24], modified algorithms such as JAYA have been adapted for power systems with various renewable resources. In [25], it is proposed a multi-objective evolutionary algorithm considering uncertainties in solar and wind power. In [26], a MO-OPF problem solution for identifying the apt trade-off between the operating cost of the generators, power loss of the system, and voltage stability index is solved using chaotic mutation and SWT combined, non-dominated sorting (NS) particle swarm optimization (SCNSPSO). In [27], researchers propose a solution technique for single and multi-objective OPF (MOOPF) issues, containing coal-based power plants plus solar and wind power plants. In [28], the proposed algorithm is implemented to tackle the MOOPF problem with wind and solar energy.

B. NOVELTY AND CONTRIBUTIONS

In the existing literature, metaheuristic algorithms have been employed using both the weighting method and the Pareto concept approach to address MOOPF problems in power systems, including the integration of renewable resources. Recently, In [29], EBOwithCMAR is introduced a new retreat phase called the Covariance Matrix Adapted Retreat Phase (CMAR), which uses the covariance matrix to generate a new solution and thus improves the local search capability of effective Butterfly Optimizer (EBO).

EBOwithCMAR is an algorithm that integrates three key components. The first component with the highest contribution is the EBO, which features a crossover operator that enhances the diversity of the population during the Perching and Patrolling processes. The second component is the CMAR, significantly contributing to the algorithm's performance. Covariance Matrix Adaptation (CMA) works by estimating the shape and direction of the search space based on the distribution of solutions. The CMAR phase is an adaptation mechanism designed to improve the search space exploration and avoid local optima. The hybrid approach is further refined by incorporating quadratic programming through Least Squares (LS). After CMAR directs the search towards promising regions, LS comes into play for fine-tuning solutions. It focuses on improving the quality of the solutions found through precise exploitation. Quadratic programming is used because it is well-suited to handle local refinement tasks where the objective function behaves quadratically or can be approximated as such. This study addresses single and MOOPF problems using the EBO, EBOCMAR, and EBOCMARLS (EBOwithCMAR) algorithms. The proposed methods use weighting approaches to minimize single and multiple objective functions applied to IEEE 30 bus test system

involving renewable energy sources. Furthermore, this research investigates and compares the effects of the EBO, CMAR, and LS components on the search speed and solution quality of the EBOwithCMAR algorithm, analyzing each objective function individually. The novelty of this study is that EBOwithCMAR and its components are separately adapted to the solution of single and multiple OPF problems. The optimum results obtained without violating the system constraints are compared with other studies in the literature. Furthermore, adapting it to system including renewable energy sources demonstrates its applicability to the solution of more complicated and complex OPF problems.

II. FORMULATION OF THE MULTI-OBJECTIVE OPF PROBLEM

A multi-objective (OPF) issue often aims to simultaneously satisfy multiple equality and inequality requirements and maximize two or more specified objective functions using optimal power system control parameters. A multi-objective optimization problem can be analytically defined as:

Optimize: $f(x,u) = [f_{Obj1}(x,u), f_{Obj2}(x,u), \dots\dots\dots, f_{ObjN}(x,u)]$

with the subject of: $g(x,u) = 0$ *and* $h(x,u) \leq 0$

where $f_{ObjN}(x,u)$ represents N^{th} is optimized the objective function. $g(x,u)$ and $h(x,u)$ are the equality constraints and the inequality constraints, respectively. In accordance with;

$$x = [P_{Gslack} V_L Q_G S_l], \quad (1)$$

where x indicates the state variables, including real generation power of the slack bus P_{Gslack}, voltage of the load bus V_L, reactive generation power Q_G and transmission line loading S_l

$$u = [P_G V_G Q_C T], \quad (2)$$

where u represents the variable vector for the elements, including the real power P_G, generator voltage V_G, the output of shunt VAR compensators Q_C and settings of the tap changing transformers T.

A. CONSTRAINTS OF THE POWER SYSTEM

In the OPF problem, finding the best fitness value of objective functions is subject to satisfying active (real) power flow and reactive power flow equations, named equality constraints. Also, security constraints on transmission lines, equipment operating limits, and voltage magnitude limits on load buses are named inequality constraints, and their details are given below.

Load Flow Equations and Constraints

The typical equations related to load flow, $g(x,u)$, in the literature is given by,

$$P_{G_i} - P_{D_i} - \sum_{j=1}^{n} |V_i||V_j||Y_{ij}| \cos(\theta_{ij} - \delta_i + \delta_j) = 0, \quad (3)$$

$$Q_{G_i} - Q_{D_i} - \sum_{j=1}^{n} |V_i||V_j||Y_{ij}| \sin(\theta_{ij} - \delta_i + \delta_j) = 0, \quad (4)$$

where P_{Gi} and Q_{Gi} are the real and reactive generation power outputs, P_{Di} and Q_{Di} are the active load and reactive load demand of bus i, the elements of the bus admittance matrix are represented by $|Y_{ij}|$ and θ_{ij} and finally n is the total bus number. The parameter constraint limits, $h(x,u,)$ including the typical load flow constraints are given as,

Generator, Transformer, Shunt Var Compensator Constraints

The generator voltage, active and reactive powers can be limited by the user as,

$$V_{Gi}^{\min} \leq V_{Gi} \leq V_{Gi}^{\max} \; i = 1, \dots\dots, N_g, \quad (5.a)$$

$$P_{Gi}^{\min} \leq P_{Gi} \leq P_{Gi}^{\max} \; i = 1, \dots\dots, N_g, \quad (5.b)$$

$$Q_{Gi}^{\min} \leq Q_{Gi} \leq Q_{Gi}^{\max} \; i = 1, \dots\dots, N_{g,} \quad (5.c)$$

where N_g defines the number of generators including the slack bus.

The maximum and minimum limits of the reactive power that can be injected or drawn by the compensators and the transformer tap settings are defined by the user as follows:

$$T_i^{min} \leq T_i \leq T_i^{max} \; i = 1, \dots\dots, N_T, \quad (6)$$

$$Q_{C_i}^{min} \leq Q_{C_i} \leq Q_{C_i}^{max} \quad i = 1, \dots\dots, N_{\mathrm{QC}}. \quad (7)$$

Security Constraints

The load bus voltage constraints and the maximum value of loadability capacity of the transmission line is,

$$V_{L_i}^{min} \leq V_{L_i} \leq V_{L_i}^{max} \quad i = 1, \dots\dots, N_{\mathrm{VL}} \quad (8)$$

$$S_{L_i} \leq S_{L_i}^{max} \quad i = 1, \dots\dots, N_{\mathrm{SL}}. \quad (9)$$

B. OBJECTIVE FUNCTIONS

This study intends to optimize the power system control parameters using the proposed EBOwithCMAR method and its parts for objective functions, including minimizing fuel cost, reducing fuel emissions, minimizing power loss, and minimizing voltage deviation. In addition, multi-objective functions were obtained by converting the above objective functions into a single objective function using the weighted sum method. The single and multi-objective functions used are listed below.

Quadratic cost(f_{CT}) and Valve point effect functions (f_{CTV}) of the thermal generators

The fuel costs regarding each generator unit are modelled by quadratic functions as:

$$f_{CT} = \sum_{i=1}^{Ng} a_i + b_i P_{Gi} + c_i P_{Gi}^2 \,. \quad (10)$$

The fuel cost functions of some generation units are either smooth (without valve point effect) or non-uniform (with valve point effect). This is due to the fluctuations caused by the opening process of the control valves of the steam turbines. Therefore, considering the valve-loading point effect, the fuel cost can be calculated using Eq. (11) [30].

$$f_{CTV} = \sum_{i=1}^{N_g} \left(a_i P_{gi}^2 + b_i P_{gi} + c_i\right) + \left| d_i \times \sin\left(e_i \times \left(P_{gi}^{min} - P_{gi}\right)\right)\right|, \quad (11)$$

where N_g is the total generator number; P_{gi} is the generation of real power at bus i ; a_i, b_i, c_i are the weighting factors, d_i and e_i are constants from the valve-point effect of the i-th generating unit.

Cost function of the wind generators(f_{CW})

The direct cost of the i-th wind power generator as a function of scheduled power is molded as following

$$C_{WD,i}(P_{Ws,i}) = g_i P_{Ws,i}\ , \quad (12)$$

where $P_{Ws,i}$ and g_i are the scheduled wind power and the direct cost coefficient related to the i-th wind power plant respectively. For the i-th wind power plant, the reserve and penalty costs are determined by:

$$C_{RW,i}(P_{Ws,i} - P_{Wav,i}) = K_{RW,i}(P_{Ws,i} - P_{Wav,i}) = K_{RW,i}\int_0^{P_{Wsj}}(P_{Ws,i} - p_{W,i})f_W(P_{W,i})dP_{W,i}, \quad (13)$$

$$C_{PW,i}(P_{Wav,i} - P_{Ws,i}) = K_{PW,i}(P_{Wav,i} - P_{Ws,i}) = K_{PW,i}\int_{P_{Ws,i}}^{P_{W,i}}(P_{W,i} - P_{Ws,i})f_W(P_{W,i})dP_{W,i}\ , \quad (14)$$

where $K_{RW,i}$ and $K_{PW,i}$ represent the reserve and penalty cost coefficients respectively, $P_{Ws,i}$ and $P_{Wav,i}$ denote the scheduled and available power, and $f_W(P_{W,i})$ is the probability density function for the $i-th$ wind power plant, any surplus power is managed by curtailing the output of conventional generators. This action requires ISO to compensate for a penalty cost associated with the unutilized power [31].

The total cost of wind power (f_{CW}) generated from wind farms is described as follows;

$$f_{CW} = \sum_{i=1}^{N_{WG}} \left[C_{WD,i}(P_{Wsij}) + C_{RW,i}(P_{Ws,i} - P_{Wav,i}) + C_{PWj}(P_{Wav,i} - P_{Ws,i})\right]. \quad (15)$$

Cost function of the Solar generators(f_{CS})

The direct cost of the k-th solar PV power generator is;

$$C_{SD,i}(P_{Ss,k}) = e_k P_{Ss,k}, \quad (16)$$

where $P_{Ss,k}$ and e_k are the scheduled PV power and the direct cost coefficient related to the k-th solar PV power plant respectively.

Like wind power plants, solar power plants also have intermittent and uncertain output. In principle, the approach to over and under-estimating solar power shall be the same as that of wind power. However, as solar radiation follows a lognormal PDF [32], different from wind distribution, which is well known for trailing Weibull PDF, for convenience in the calculation, the reserve and penalty cost models are built based on the concept presented in [33].

Reserve and cost Penalty for the k-th solar PV plant is:

$$C_{Rs,k}(P_{ss,k} - P_{sav,k}) = K_{Rs,k}(P_{ss,k} - P_{sav,k}) = K_{Rs,k} * f_s(P_{sav,k} < P_{ss,k}) * [P_{ss,k} - E(P_{sav,k} < P_{ss,k})] \quad (17)$$

$$C_{PS,k}(P_{Sav,k} - P_{Ss,k}) = K_{PS,k}(P_{Sav,k} - P_{Ss,k}) = K_{PS,k} * f_S(P_{Sav,k} > P_{Ss,k}) * [E(P_{Sav,k} > P_{Ss,k}) - P_{Ss,k}]. \quad (18)$$

where $K_{RS,k}$ and $K_{PS,k}$ are the reserve and penalty cost coefficients for the k-th solar PV plant, $f_s(P_{Sav,k} < P_{Ss,k})$ and $E(P_{Sav,k} < P_{Ss,k})$ denote the respective probabilities and expectations of power shortages and surpluses $f_s(P_{Sav,k} > P_{Ss,k})$ and $E(P_{Sav,k} > P_{Ss,k})$ relative to the scheduled power output ($P_{Ss,k}$).The total cost of solar (f_{CS}) generated from solar panels is described as follows;

$$f_{CS} = \sum_{k=1}^{N_{SG}} \left[C_{SD,k}(P_{Ss,k}) + C_{RS,k}(P_{Ss,k} - P_{Sav,k}) + C_{PS,k}(P_{Sav,k} - P_{Ss,k})\right] \quad (19)$$

***Cost function* of the Hydro power generator (f_{CH})**

The direct cost of the j-th hydro power generator is as follows;

$$C_{HD,j}(P_{Hs,j}) = f_k P_{Hs,j} \quad (20)$$

where $P_{Hs,j}$ and f_j show the scheduled hydro power and the direct cost coefficient related with the j-th hydro power generator, respectively.

The reserve and penalty cost of the cost of the j-th hydro power generator is shown as follows [34]:

$$C_{RH,j}(P_{Hs,j} - P_{Hav,j}) = K_{RH,j}(P_{Hs,j} - P_{Hav,j}) = K_{RH,j} * f_H(P_{Hav,j} < P_{Hs,j}) * [P_{Hs,j} - E(P_{Hav,j} < P_{Hs,j})]\ . \quad (21)$$

$$C_{PH,j}(P_{Hav,j} - P_{Hs,j}) = K_{PH,j}(P_{Hav,j} - P_{Hs,j}) = K_{PH,j} * f_H(P_{Hav,j} > P_{Hs,j}) * [E(P_{Hav,j} > P_{Hs,j}) - P_{Hs,j}]\ , \quad (22)$$

where $K_{RH,j}$ and $K_{PS,k}$ represent the reserve and penalty cost coefficients for the j-th hydropower generator, respectively, $f_H$and E denote the probability and expectation of hydro power shortages $f_H(P_{Hav,j} < P_{Hs,j})$, $E(P_{Hav,j} < P_{Hs,j})$and surpluses $f_H(P_{Hav,j} > P_{Hs,j})$, $E(P_{Hav,j} > P_{Hs,j})$ relative to the scheduled power $P_{Hs,j}$.

The total cost (f_{CH}) of hydro power generator is presented as in the following;

$$f_{CH} = \sum_{k=1}^{N_{HG}} \left[C_{HD,j}(P_{Hs,j}) + C_{RH,j}(P_{Hs,j} - P_{Hav,j}) + C_{PH,j}(P_{Hav,j} - P_{Hs,j})\right]. \quad (23)$$

Fuel cost emission (f_E)

To satisfy increasing energy demand, it is inevitable to generate electrical energy despite harmful gas emissions and worsening air pollution. Therefore, fuel emission optimization aims to minimize the number of harmful gases released into the atmosphere by optimizing the system's control variables.

$$f_E = \sum_{i=1}^{N_g} \alpha_i + \beta_i P_{Gi} + \gamma_i P_{Gi}^2 + \xi_i\, exp(\lambda_i P_{Gi})), \quad (24)$$

where f_E is the total emission cost (ton/h) expressed in tons per hour (ton/h), and the coefficients α_i, β_i, γ_i, ξ_i and λ_i are unit-specific emission parameters; the exponential term accounts for non-linear emission behavior due to load variations.

Transmission real power losses (f_{PL})

The real power losses for each transmission line can be calculated as,

$$f_{PL} = \sum_{i=1}^{N_L} g_i[V_k^2 + V_m^2 - 2V_kV_m\, cos(\delta_k - \delta_m)], \quad (25)$$

where N_L is the number of transmission lines; g_i is the conductance of the ith line; V_k and V_m are the voltage magnitude at the end buses k and m of the ith line, respectively, and δ_k and δ_m are the voltage phase angle at the end buses k and m.

Voltage Deviation (f_{VD})

In order to improve the voltage profile of the system, the voltage values of all load buses at 1 p.u should be fixed by

minimizing the voltage deviation [16]. To calculate the voltage deviation for load buses, use the following formula:

$$f_{VD} = \sum_{i=1}^{N_{PQ}} |V_i - 1|. \quad (26)$$

where N_{PQ} is the load bus number.

Multi–Objective functions of without renewable energy source

The equation below can minimize the generation cost and loss and (J_1) and the generation cost and voltage deviations(J_2) simultaneously.

$$J_1 = f_{CT} + \lambda_1 f_{PL}, \quad (27)$$

$$J_2 = f_{CT} + \lambda_2 f_{VD}, \quad (28)$$

where λ is a scaling factor to balance between the objective function values and avoid an objective's dominance over another. In this paper λ_1 is selected as 40 [18] and λ_2 is selected as 100 [17].

Multi–Objective functions of renewable energy source (J_3)

The new objective functions, which seek to minimise the cost functions of renewable energy sources by integrating them with the cost functions of thermal generators, can be articulated as follows.

$$J_3 = f_{CTV} + f_{CW} + f_{CS} \quad (29.a)$$
$$J_4 = f_{CTV} + f_{CW} + f_{CS} + C_{tax} f_E \quad (29.b)$$

For the system that integrates hydro energy sources,

$$J_5 = f_{CT} + f_{CW} + f_{CS} + f_{CH}, \quad (30.a)$$
$$J_6 = f_{CTV} + f_{CW} + f_{CS} + f_{CH}, \quad (30.b)$$
$$J_7 = f_{CT} + f_{CW} + f_{CS} + f_{CH} + C_{tax} f_E. \quad (30.c)$$

In this study, the C_{tax} is set at 20 USD/ton [35].

III. EFFECTIVE BUTTERFLY OPTIMIZER WITH COVARIANCE MATRIX ADAPTED RETREAT PHASE (EBO WITH CMAR)

A. EBO

EBO is a dual population-based bio-inspired optimization method that draws inspiration from male butterfly mate-locating behaviors [36]. Random initial populations serve as the foundation for EBO, which are $X_1 = \{\bar{x}1_1, \bar{x}1_2, \dots, \bar{x}1_{PS_1}\}$ and $X_2 = \{\bar{x}2_1, \bar{x}2_2, \dots, \bar{x}2_{PS_2}\}$, with PS_1 and PS_2 denoting the corresponding population sizes of the primary and secondary populations. Vectors $\bar{x}1_z$ and $\bar{x}2_z$'s components have to fall within the searching region. Following the "criss-cross" or "towards-best" change, a new population, $V = \{\bar{v}_1, \bar{v}_2, \dots, \bar{v}_{PS_1}\}$, is created. As a result, each $\bar{x}1_z$ is crossed with its matching $\bar{v}_z$ to produce an example vector $\bar{s}_z$. For each of these pairings, a pair-wise assessment between $\bar{x}1_z$ and $\bar{s}_z$ is performed using the fitness values. The samples that perform better in the pairwise evaluation make up the primary population set, while the remainder vectors are placed in the secondary population set. A brief description of each phase and operator listed above can be found in [29].

A concise introduction to the EBO technique was covered in the preceding discussion. EBO with CMAR controls several parameters of EBO, which are PS_1, cross − over (CR) [37], F *and* T to boost the variety of the general population, and through the use of the self-adaptive mechanism. The parameter F, a positive real number, is proportional to the rate of the population's evolution, while T is a real number within the interval [0, 0.5]. The crossover technique reduces to the standard binomial crossover for the specific case where $T = 0$. In accordance with the declaration made earlier, EBO is first set up with two populations, namely PS_1 and PS_2, which have been selected at random from the whole population X. Two novel modification equations are used in EBO for the purpose of patrolling and perching, respectively, while this work is performed. The following is a description of the improved stages of EBO, which were introduced in the original paper [29].

Perching and Patrolling Phase

The solution update equations are defined in perching and patrolling search phases in Eq. (31) and Eq. (32) respectively where the crossover probability vector, cr_j, is computed for each solution using *cross_over_probs( )* function.

$$v_{z,j} = \begin{cases} x_{z,j} + F_z\left(x_{r1_z,j} - x_{z,j} + x_{r2_z,j} - allX_{r3,j}\right), \\ \text{if } \left(rand_j\ (0,1) \le cr_{z,j} \text{ or } j = j_{rand}\right) \\ x_{z,j}, \\ \text{otherwise.} \end{cases} \quad (31)$$

$$v_{z,j} = \begin{cases} x_{z,j} + F_z\left(x_{\text{best}_z,j} - x_{z,j} + x_{r1_z,j} - x_{r2_z,j}\right), \\ \text{if } \left(rand_j\ (0,1) \le cr_{z,j} \text{ or } j = j_{rand}\right) \\ x_{z,j}, \\ \text{otherwise.} \end{cases} \quad (32)$$

where the $allX$ variable is defined in the algorithm, and $r1_z$, $r2_z$ and $r3_z$ are distinct integers. The $best_z$ is the index of the best individual among the randomly chosen D individuals if the population size PS is greater than $2D$. Otherwise, it is the best of the randomly chosen 10% individuals.

Calculation of $prob_{perch}$ and $prob_{pat}$

The initial values of the probabilities $prob_{perch}$ and $prob_{pat}$ are set to 0.5 and later computed using *calculate_probs( )* function according to the improvement rate in objective function values, formulated through Eqs. (33), (34). The improvement rate is evaluated separately for solutions updated during the perching phase (denominator index = 1) and the patrolling phase (index = 2), normalized by the initial probability value:

$$I_i^{t+1} \frac{\sum_{z=1,i}^{PS_1} max\left(0, f_z^{t+1} - f_z^t\right)}{\sum_{z=1,i}^{PS_1} f_z^t} \text{ where } \forall x_z \text{ updated by } \begin{cases} \text{perching,} & \text{if } i = 1 \\ \text{patrolling,} & \text{if } i = 2. \end{cases} \quad (33)$$

Then, $prob_{perch}$ and $prob_{pat}$ are calculated as follows;

$$prob_{perc} = max\left(0.1, min\left(0.9, \frac{I_1}{I_1 + I_2}\right)\right). \quad (34)$$

Linear Reduction of Population

Population size PS is reduced linearly at the end of each iteration by eliminating some worst solutions in X and $fitX$ according to fitness values. Here, $fitX$ is the vector of objective function values of the solutions in X. The new pop size PS^{t+1} is computed using Eq. (35) [38].

$$PS^{t+1} = round\left(\left(\frac{PS_{min} - PS_{max}}{FE_{max}}\right) * cFE\right) + PS_{max} \quad (35)$$
$$[X, fitX] = remove_worst_K_solutions(X, fitX, K)$$

where PS_{min}, PS_{max} are the minimum and maximum pop sizes respectively, FE_{max} and cFE are the maximum number of function evaluations and current total function evaluations respectively, and K, which is, $K = PS - PS^{t+1}$, is the number of worst solutions to remove from *X* and *fitX*.

Adaptation of F, $Freq$, CR and T

For parameters $Freq$, CR and T, SHBA is used to sample new parameter setting accordingly with [39]. New parameter setting, CR_z, F_z, Freq_z, and T_z, associated with individual x_z, are calculated by Eq. (36) respectively.

$$\begin{aligned} CR_z &= M2(M_{CR,r}, 0.1), \\ F_z &= randci\,(M_{F,r}, 0.1), \\ freq_z &= randci\,(M_{CR,r}, 0.1), \\ T_z &= M2(M_{T,r}, 0.05), \end{aligned} \quad (36)$$

where M_{param} is the memory vector for param ϵ $\{CR, F, Freq, T\}$ and r is random integer from $[1, memSize]$, *randci* is the cauchy distributions and *M2* is the multi-variate random distribution around the mean M_{param}, r and symmetric covariances with deviations given.

B. COVARIANCE MATRIX ADAPTED RETREAT (CMAR)

New solutions are sampled from a random distribution by computing a mean and covariance matrix, and these new individuals are then weighted according to their objective function value. A subset of these individuals is selected to form a new population, which is used to compute the mean and covariance matrix for the subsequent iteration. Detailed information with a brief description of each step to create the example solution is provided in [40]. Additionally, the explanations on the self-adaptation of the covariance matrix and the calculation of the step size can be found in [41].

C. FRAMEWORK OF THE EBO WITH CMAR

The EBOwithCMAR algorithm, inspired by the structure of UMOEAs-II [42], begins by generating a random initial population that is divided into three subpopulations. The first two are used by EBO, and the third by CMAR.

During optimization, the algorithm alternates between EBO and CMAR based on two dynamically changing probabilities $prob_1$ and $prob_2$ [42]. Each cycle runs both methods concurrently for half its duration, then updates the probabilities according to the quality of their best solutions and the relative sizes of their subpopulations. After each cycle, the probabilities are reset, and the process repeats.

To enhance local exploitation, a Sequential Quadratic Programming (SQP) procedure is introduced after 75% of the optimization process, using an adaptive probability $prob_{ls}$ [42]. If SQP finds a better solution, its probability is reset; otherwise, it is reduced. The process continues until the stopping criterion is met.

The probabilities $prob_1$ and $prob_2$ are updated based on each algorithm's solution quality and population diversity. Normalized quality and diversity values are calculated at mid-cycle, then combined into a progress index (PI). Each probability is derived by normalizing these indices, constrained between 0.1 and 0.9. If both indices are zero, the probabilities default to one. The algorithm with the higher probability at the end of a cycle is considered more effective and influences population exchange and parameter resetting for the next cycle [42].

Algorithm EBO with CMAR

Define $PS \leftarrow PS_1 + PS_2 + PS_3, Cy \leftarrow 0,\ prob_1 = prob_2 \leftarrow 1$ and all necessary parameters
for $i = 1{:}PS$ **do**
    $X_i \leftarrow D$ random numbers that are uniformly distributed
end for
Assign PS_1, PS_2, and PS_3 individuals in a random manner from X to X_i, $\forall i = 1, 2, 3$
while termination criterion is not met **do**
    $cy \leftarrow cy + 1$
    if $cy == \frac{CS}{2}$ **then**
        Compute $prob_1$ and $prob_2$
    end if
    if $cy == CS$ **then**
        Share Data
        $prob_1 = 1$, and $prob_2 = 1$
        $cy \leftarrow 0$
    end if
    if $rand(0,1) \leq prob_1$ **then**
        Perform EBO
        $cFE \leftarrow cFE + PS_1$
    end if
    if $rand(0,1) \leq prob_2$ **then**
        Perform CMAR
        $cFE \leftarrow cFE + PS_1$
    end if
    if $rand(0,1) \leq prob_{ls}$ & $cFE \geq 0.75 * FE_{max}$ **then**
        Perform SEQ
        $cFE \leftarrow cFE + FE_{seq}$
        if best solution is improved **then**
            $prob_{ls} \leftarrow 0.1$
            Update X_1 and X_2
        else
            $prob_{ls} \leftarrow 0.0001$
        end if
    end if
    $t \leftarrow t + 1$
end while
until X

IV. RESULTS AND DISCUSSION

The feasibility and effectiveness of the proposed hybrid EBOwithCMAR and its parts, such as called EBO and EBOCMAR, for solving single objective OPF (SOOPF) and MOOPF problems are tested on IEEE 30-bus test system. Table 1 presents the data, specifications, and minimum and maximum operating constraints for test system. Further details can be found in [43,44]. For the IEEE 30 bus test system, the lower and upper limits of load bus voltage magnitudes are set at [0.95 - 1.05] p.u., whereas the lower and upper limits of generator bus voltage magnitudes are set at [0.9 - 1.1] p.u., respectively. We applied the penalty technique to ensure that test system and

control variables remained within the acceptable ranges specified. 10 cases were examined across IEEE test system, as summarized in Table 2. A tick mark has been placed in the Table 2 for the specified case studies. Each test case is experimented with the proposed algorithms, each using a population size of 30 and a maximum iteration of 10,000. Graphical comparisons are also presented to investigate the convergence performance of EBO, EBOCMAR (EBOwithCMAR without LS), and EBOCMARLS. The results show that all constraints strictly adhere to the acceptable ranges when the algorithms converge.

Table 1. IEEE 30 bus test system

Items	IEEE 30 Bus Test System		
	Quantity	Description	Range
Buses	30	[43]	
Branches	41	[14]	
V_G [p.u]	6	Buses:1(Slack),2,5,8,11,13	[0.95 1.1]
Q_C [MVar]	9	Buses:10,12,15,17,20,21,23,24,29	[0.0 5 .0]
T [pu]	4	Branches:11, 12, 15, 36	[0.95 1.1]
V_L [p.u]	24		[0.95 1.05]
Control variables	24	Without renewable [P_G, V_G, Q_C, T] with renewable [P_G, V_G, T]	

Table 2. Summary of case studies on test system

IEEE 30 bus system									
	Without renewable				Renewable				
	f_{CT}	f_E	f_{Pl}	f_{VD}	f_{CTV}	f_{CW}	f_{CS}	f_{CH}	f_E
Case 1	✓								
Case 2		✓							
Case 3			✓						
Case 4	✓		✓						
Case 5	✓			✓					
Case 6					✓	✓	✓		
Case 7					✓	✓	✓		✓
Case 8	✓					✓	✓	✓	
Case 9					✓	✓	✓	✓	
Case 10	✓					✓	✓	✓	✓

A. IEEE 30 BUS TEST SYSTEM

The system demand for active power was 2.834 p.u., and for reactive power was 1.262 p.u. at a base of 100 MVA. There are six thermal generators on busbars 1,2,5,8,11, and 13. The coefficients for the fuel cost are available in [14]. There are nine fixed capacitors in the system where renewable energy sources are not integrated, and two fixed capacitors on busbars 10 and 24 in the system where they are integrated [45]. In this section, 7 cases are studied. In the first 5 case studies, renewable energy sources are not incorporated into the system. In case studies 6 and 7, two wind farms and one solar system are integrated into the IEEE 30 bus test system instead of thermal generators 5-11 and 13, respectively [33]. In cases 8,9 and 10 which integrated hydro energy source, the thermal generators at buses 8 and 13 have been replaced with a wind energy source and a combined hydro and wind energy source, respectively. Additionally, a PV unit was installed at bus 11.

Case Studies Without Renewable Energy Sources

The EBO, EBOCMAR, and EBOCMARLS approaches were employed to solve SOOPF and MOOPF Optimal Power Flow problems on the IEEE 30-bus test system. In the initial case study, the objective was to minimize the total fuel cost of the thermal generators, as calculated by Eq. (10). In Fig. 1(a), CMAR part has made an effective search to minimize the cost function. Still, EBO alone has found the solution points that give the smallest value by reaching 800.3873 $/h. EBOCMARLS has been fails to provide a high-quality solution for a simple quadratic objective function due to the influence of the LS part. However, EBO outperforms them and achieves the best optimum value.

In Case 2, it is aimed to minimize the emission release by thermal generators. EBO, EBOCMAR and EBOCMARLS have managed to reduce the emission value to 0.2048 ton/h. In Case 3, the SOOPF problem is solved by minimizing the active power loss. As can be seen from Table 3, EBOCMAR reached the lowest value with 3.0777 MW. EBO and EBOCMARLS found the same optimum value with 3.0779 MW values. In the multi-objective optimal power flow problem formulated in Eq. (27), the aim is to minimize the sum of active power loss and fuel cost. In this target function, we see the effect of the search and discovery ability of the CMAR part. The combined effect of CMAR and LS ensures that the optimization process is both robust in exploration and refined in exploitation.

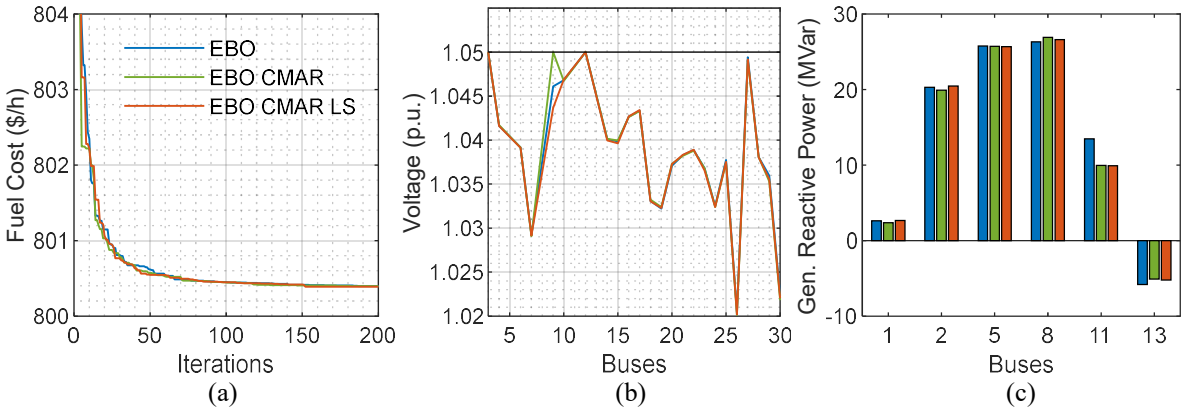

Figure 1. Fuel cost optimization for (a) Convergence curve (b) voltage profile (c) generator reactive power output.

When Fig. 2 is examined, it is seen that the CMAR and LS parts are not stuck in local optima and have continuously searched to find the best solution point throughout the optimization process. In addition, it has increased the convergence speed of EBO. In this case, it is aimed to minimize the total fuel cost of thermal generators and the sum of voltage deviations in load bars simultaneously. The value of the target function is calculated with equation in Eq. (28). The results of the control variables are given in Table 4. While EBO alone managed to minimize the active power loss, the search for better solution points of CMAR and LS parts to minimize the voltage deviation yielded positive results. While EBO succeeds in reducing the value of the sum of the two objective functions to 812.9074 as shown in Figure 2.a, it is seen that the CMAR part prevents premature convergence.

Table 3. Simulation results of case 1-3 on IEEE-30 bus standard test system for SOOPF

Items	Range	Case-1			Case-2			Case-3		
		EBO	EBOCMAR	EBO CMAR LS	EBO	EBO CMAR	EBO CMAR LS	EBO	EBO CMAR	EBO CMAR LS
P_1	[80 250]	177.1638	177.1114	177.1808	64.0484	64.0738	64.0514	51.4783	51.4810	51.4783
P_2	[20 80]	48.7201	48.7269	48.7593	67.5623	67.5376	67.5594	79.9997	79.9976	79.9999
P_5	[15 50]	21.3912	21.3795	21.3942	50	50	49.9999	49.9998	49.9999	49.9999
P_8	[10 35]	21.2044	21.2181	21.1511	35	34.9999	35	34.9999	34.9999	34.9999
P_{11}	[10 30]	11.9175	11.9580	11.9139	30	29.9999	29.9999	29.9999	29.9996	29.9999
P_{13}	[12 40]	12.0002	12.0001	12.0010	40	39.9999	39.9999	39.9999	39.9995	39.9997
V_1	[0.95 1.1]	1.0833	1.0830	1.0834	1.0624	1.0623	1.0624	1.0614	1.0615	1.06142
V_2	[0.95 1.1]	1.0443	1.0440	1.0444	1.0265	1.0064	1.0167	1.0172	1.0274	1.0273
V_5	[0.95 1.1]	1.0332	1.0330	1.0331	1.0370	1.0373	1.0373	1.0378	1.0381	1.0378
V_8	[0.95 1.1]	1.0478	1.0480	1.0478	1.0539	1.0534	1.0541	1.0540	1.0543	1.0542
V_{11}	[0.95 1.1]	1.0720	1.0690	1.0628	1.0553	1.0560	1.0568	1.0482	1.0591	1.0503
V_{13}	[0.95 1.1]	1.0420	1.0430	1.0428	1.0566	1.0513	1.0522	1.0535	1.0488	1.0542
$Q_{c\text{-}10}$	[0 5.0]	0.4698	2.3321	3.4721	0.1316	0.0631	1.0490	2.7242	0.1209	2.3815
$Q_{c\text{-}12}$	[0 5.0]	2.6104	2.4939	2.2847	0.0017	4.7626	1.7621	2.2730	4.5740	1.2723
$Q_{c\text{-}15}$	[0 5.0]	4.3790	4.5048	4.0360	4.1070	4.0327	4.7747	4.5912	4.3180	4.0429
$Q_{c\text{-}17}$	[0 5.0]	4.9991	4.9997	4.9991	4.9999	4.9980	4.9968	4.9682	4.9994	4.9979
$Q_{c\text{-}20}$	[0 5.0]	4.0735	4.2208	4.2168	4.3312	4.4954	3.9900	4.1371	4.2238	4.4193
$Q_{c\text{-}21}$	[0 5.0]	4.9999	4.9984	4.9983	4.9955	4.9964	4.9999	4.9950	4.9969	4.9997
$Q_{c\text{-}23}$	[0 5.0]	3.3006	3.2943	3.2390	3.1906	2.9786	3.1191	3.1050	3.2964	3.3764
$Q_{c\text{-}24}$	[0 5.0]	4.9999	4.9993	4.9999	4.9999	4.9997	4.9996	4.9999	4.9981	4.9998
$Q_{c\text{-}29}$	[0 5.0]	2.0158	1.9338	1.9662	1.9768	1.9384	1.7658	1.9431	1.8812	1.8684
T_{11}	[0.9 1.1]	1.0180	1.0002	1.0183	1.0410	1.0353	1.0451	1.0463	1.0431	1.0480
T_{12}	[0.9 1.1]	0.9331	0.9594	0.9355	0.9020	0.9087	0.9009	0.9007	0.9021	0.9000
T_{15}	[0.9 1.1]	0.9639	0.9655	0.9640	0.9898	0.9912	0.9877	0.9905	0.9880	0.9893
T_{16}	[0.9 1.1]	0.9714	0.9717	0.9715	0.9749	0.9736	0.9732	0.9742	0.9746	0.9742
Q_1	[-20 150]	2.6436	2.3505	2.6611	-5.1827	-5.2530	-5.4104	-5.2434	-5.2282	-5.4578
Q_2	[-20 60]	20.3034	19.9425	20.4788	7.6385	7.5030	7.8979	7.2494	7.3177	7.47559
Q_5	[-15 62.5]	25.7590	25.7307	25.6842	21.5223	22.0249	21.6673	21.7869	21.8246	21.6337
Q_8	[-15 48.7]	26.3386	26.9330	26.6033	26.8253	25.9197	26.5321	26.1413	26.2934	26.2961
Q_{11}	[-10 40]	13.4822	9.9406	9.9030	10.6522	10.2688	11.5862	8.5807	12.1580	9.5092
Q_{13}	[-15 44.7]	-5.7896	-5.0821	-5.2025	6.0468	2.0074	2.6985	3.6863	0.1280	4.2428
f_{CT}($/h)		**800.3873**	800.3878	800.3877	944.3125	944.2736	944.3079	967.6085	967.6025	967.6088
f_E(ton/h)		0.3663	0.3662	0.3664	**0.2048**	**0.2048**	**0.2048**	0.2073	0.2073	0.2073
f_{Pl} (p.u)		8.9975	8.9942	9.0005	3.2108	3.2114	3.2109	3.0779	**3.0777**	3.0779

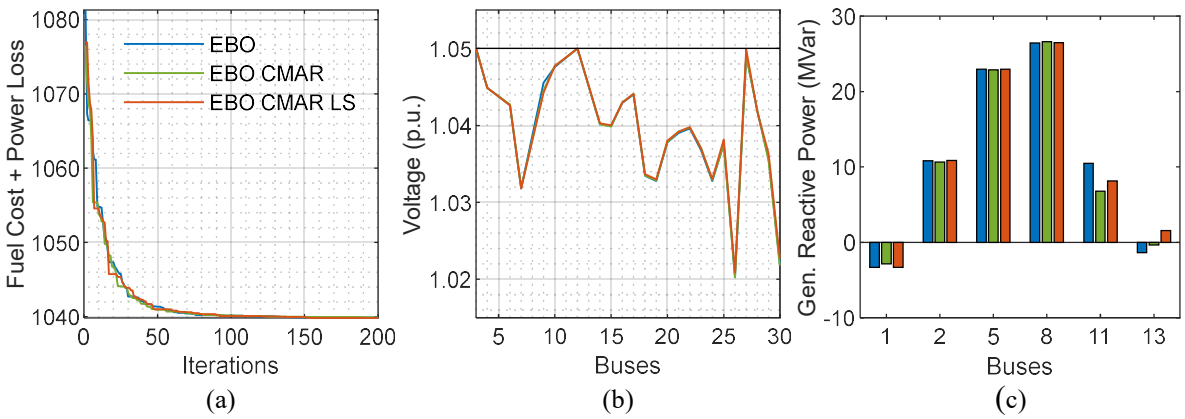

Figure 2. Fuel cost with power loss optimization for (a) Convergence curve (b) voltage profile (c) generator reactive power output.

Table 4. simulation results of case 4-5 on IEEE-30 bus standard test system for MO-OPF

Items	Range	Case-4			Case-5		
		EBO	EBOCMAR	EBOwithCMAR	EBO	EBOCMAR	EBOwithCMAR
P_1	[80 250]	102.5503	102.8145	102.5723	176.5169	176.5939	176.7009
P_2	[20 80]	55.60443900	55.56454500	55.63384000	48.76358100	48.84255700	48.80625000
P_5	[15 50]	38.11838600	38.01823800	38.11515900	21.63094000	21.59851600	21.77208600
P_8	[10 35]	34.99999200	34.99571700	34.99997800	22.02853000	21.89840500	21.63470300
P_{11}	[10 30]	29.99998500	29.99648700	29.99979200	12.25464500	12.27982400	12.31241100
P_{13}	[12 40]	26.64691400	26.54290200	26.60030000	12.00342400	12.00117200	12.00152900
V_1	[0.95 1.1]	1.068680800	1.068966600	1.068691600	1.045193000	1.043489500	1.043896700
V_2	[0.95 1.1]	1.018031900	1.018117200	1.008041900	0.9966059300	0.9865570600	1.007237900
V_5	[0.95 1.1]	1.034682300	1.034634500	1.034659800	1.024032200	1.013950400	1.014975300
V_8	[0.95 1.1]	1.052753200	1.052909900	1.052751200	1.0110	1.020190500	1.011115700
V_{11}	[0.95 1.1]	1.064395400	1.056276000	1.058626200	1.021214000	1.030119900	1.018222200
V_{13}	[0.95 1.1]	1.047578100	1.048916500	1.051462600	0.9878025700	0.9884062600	0.9883547800
$Q_{c\text{-}10}$	[0 5.0]	0.3544150000	3.927905300	2.468415800	4.998666100	4.990778500	4.729315900
$Q_{c\text{-}12}$	[0 5.0]	3.836119800	2.235211600	0.7821905700	0.6206225600	0.4409082900	0.9382570600
$Q_{c\text{-}15}$	[0 5.0]	4.352705200	4.077746200	4.437261500	4.999566800	4.999940900	4.949246900
$Q_{c\text{-}17}$	[0 5.0]	4.999956200	4.960535500	4.999870500	0.00046924472	0.00035863328	0.00065826499
$Q_{c\text{-}20}$	[0 5.0]	4.173094000	4.180544600	4.256591300	4.999992500	4.999834900	4.982208300
$Q_{c\text{-}21}$	[0 5.0]	4.999458100	4.999993300	4.999861500	4.995139000	4.990319100	4.998451600
$Q_{c\text{-}23}$	[0 5.0]	3.176911400	3.443079000	3.147709000	4.999982000	4.994842700	4.990971900
$Q_{c\text{-}24}$	[0 5.0]	4.999998100	4.998671200	5	4.999716700	4.999972200	4.999813700
$Q_{c\text{-}29}$	[0 5.0]	1.992434500	1.961334800	1.979093800	2.620771900	2.604576100	2.643744200
T_{11}	[0.9 1.1]	1.016408400	1.012514900	1.015891600	1.037039300	1.047000500	1.033433200
T_{12}	[0.9 1.1]	0.9295422100	0.9403137700	0.9331412900	0.9000538500	0.9000351800	0.9002926400
T_{15}	[0.9 1.1]	0.9812030200	0.9797507900	0.9812020900	0.9394240900	0.9400631700	0.9401094100
T_{16}	[0.9 1.1]	0.9727827900	0.9731950000	0.9717948100	0.9706939100	0.9705900300	0.9706546600
Q_1	[-20 150]	-3.33280	-2.8493	-3.3293	2.679302400	-1.1866	-1.4889
Q_2	[-20 60]	10.82706200	10.64298700	10.85197800	15.24343300	18.07143200	19.35188900
Q_5	[-15 62.5]	22.97394500	22.86347300	22.94877600	46.14481800	45.96501400	46.75514600
Q_8	[-15 48.7]	26.43056200	26.59856200	26.46349100	30.28739200	27.39078900	30.84729600
Q_{11}	[-10 40]	10.47707500	6.792054900	8.153648300	10.56813400	15.06878700	9.072533500
Q_{13}	[-15 44.7]	-1.36060	-0.3617	1.546797400	-14.7469	-14.3217	-14.5002
f_{CT}($/h)		859.0432	858.5683	858.9914	803.4714	803.4926	803.5331
f_{Pl}MW)		4.5203	4.5324	4.5212	9.7980	9.8143	9.8278
f_{VD}(p.u)		0.9385	0.9379	0.9422	0.0944	0.0942	0.0940
J_1		1039.8552	1039.8632	**1039.8394**			
J_2					**812.9074**	812.9107	812.9317

Case Studies with Wind and Solar Energy Sources

In this section, the wind generators are planned to be replaced in IEEE 30 bus power system instead of thermal generators in buses 5 and 11. The output of the solar PV unit at bus 13 is dependent upon solar radiation and is represented by a lognormal probability density function (PDF) function. For

predicting the wind power depending on the wind speed, Weibull used PDF. The Weibull PDF has 2 parameters namely c and k which are scale and shape factor, respectively. In order to employ the probability of wind speed v m/s by using Weibull PDF, in Eq. (37) is given below where $f_v(v)$ is the wind speed probability.

$$f_v(v) = \left(\frac{k}{c}\right).\left(\frac{v}{c}\right)^{(k-1)}.e^{-(v/c)^k} \ \{0 < v < \infty\}. \quad (37)$$

Also, in order to present the Weibull PDF of wind farm, the parameters of v_{in}, v_r and v_{out} which are cut-in, rated and cut-out speed should be determined. The output of the solar PV unit at bus 13 is dependent upon solar radiation and is represented by a lognormal PDF function. The probability of solar irradiance (G) following lognormal PDF with mean μ and standard deviation σ is:

$$f_G(G) = \frac{1}{G\sigma\sqrt{2\pi}} exp\left\{\frac{-(ln\ x-\mu)^2}{2\sigma^2}\right\} \text{ for } G > 0. \quad (38)$$

Mean of lognormal distribution is defined as:

$$M_{lgn} = exp\ \left(\mu + \frac{\sigma^2}{2}\right). \quad (39)$$

A Monte Carlo simulation with 10,000 iterations is employed to determine the probability distributions of wind speed and solar irradiance at buses 5, 11, and 13. This simulation utilizes the parameters for the Weibull and Lognormal PDFs, in addition to the direct cost, reserve cost, and penalty coefficients provided in Table 5.

Table 5. PDF parameters for stochastic models of wind and solar energy sources

Bus	P_R [MW]	v_{in}, v_r, v_{out} [m/s]	c, k	g	K_{RW}, K_{PW}	G[W/m^2]	μ, σ	h	K_{RS} , K_{PS}
5(wind)	75	3, 16, 25	9, 2	1.6	3 1.5				
11(Wind)	60	3, 16, 25	10, 2	1.75	3 1.5				
13(PV)	50					483	0.6, 0.06	1.6	3, 3

Case 6 performs optimization of generation schedule for all thermal and renewable source generators to minimize total generation cost given by Eq. (29.a). Detailed optimal results of control and status variables obtained by EBO, EBOCMAR and EBOCMARLS are given in Table 6. EBOCMARLS achieved the lowest production cost at $781.0729 /h and is highlighted in bold. In Fig. 3.a, we can see that EBO while trying to converge quickly, it gets stuck at the local minimum point and then escapes from this point. It is clear that the effect of the discovery and search capabilities of the CMAR and LS parts is quite effective for this function. LS enhances the precision and accuracy of the final solutions by applying a more focused search while CMAR ensures that once a promising region has been explored by CMAR, the solutions are fully optimized.

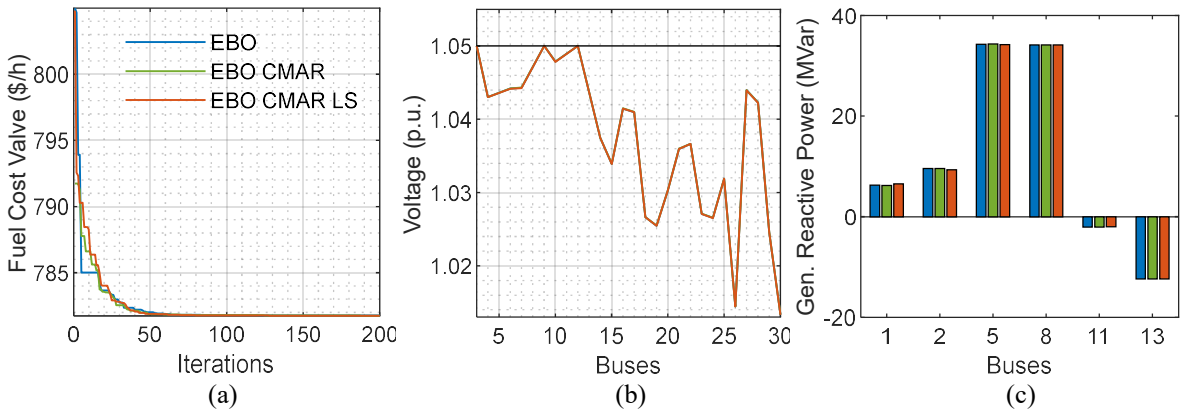

Figure 3. Fuel cost valve with renewable optimization for (a) Convergence curve (b) voltage profile (c) generator reactive power output.

In case 7 minimizes the total generation cost that includes carbon tax imposed on the emission from conventional thermal power generators. The cumulative cost, given by Eq. (12), As wind and solar power are clean form of energy, the penetration of these sources is expected to increase due to the carbon tax component. Optimum valuables of the control variables, generator reactive power, total generation cost (including carbon tax) and other calculated parameters are listed in Table 6. EBO, EBOCMAR and EBOCMARLS have managed to bring this target function, which is the sum of the valve effective cost and fuel emission values, to the value of 808.7237. Table 7 shows the results of the comparing to earlier studies in 30-bus system for cases 1-5. In addition, Table 10 presents the comparison results with previous studies in the 30-bus system with integrated renewable energy sources for cases 6-7-8-9 and 10.

Table 6. Simulation results of case 6-7 on IEEE-30 bus system for renewable system

Items	Range	Case-6			Case-7		
		EBO	EBOCMAR	EBOwithCMAR	EBO	EBOCMAR	EBOwithCMAR
P_1	[80 250]	134.9079	135.0260	135.0245	125.6208	125.6205	125.6199
P_2	[20 80]	28.85885	28.86918900	28.83382800	33.51335800	33.51218300	33.51052800
P_{5wind}	[0 75]	43.69028	43.79561100	43.88645600	46.24647000	46.24638800	46.25050200
P_8	[10 35]	10.00002	10.00011700	10.00010700	10	10	10.100
P_{11wind}	[0 60]	36.98909	37.09850900	37.04018200	38.98783500	38.98928200	38.98728200
$P_{13solar}$	[0 50]	34.42959	34.42953800	34.43017100	34.42937600	34.42937800	34.42955300
V_1	[0.95 1.1]	1.079396	1.082256100	1.082341300	1.081311100	1.081311100	1.081315100
V_2	[0.95 1.1]	1.023908	1.046096700	1.046053100	1.046332800	1.046332600	1.046325700
V_5	[0.95 1.1]	1.071125	1.062629700	1.062498500	1.063387100	1.063386400	1.063394300
V_8	[0.95 1.1]	1.054610	1.054274800	1.054238900	1.054634500	1.054634500	1.054633900
V_{11}	[0.95 1.1]	1.058946	1.044400700	1.044452400	1.044030500	1.044030600	1.044031300
V_{13}	[0.95 1.1]	1.047794	1.032895200	1.032870900	1.032822800	1.032822900	1.032823400
Q_{TG1}	[-20 150]	6.249839800	6.217253200	6.515364200	5.916863300	5.917218100	5.940349200
Q_{TG2}	[-20 60]	9.595135500	9.551554500	9.341847800	9.214691500	9.214681200	9.179273600
Q_{WG1}	[-30 35]	34.24810000	34.33930000	34.20780000	34.97160000	34.97110000	34.98230000
Q_{TG8}	[-15 48.7]	34.16394300	34.15979600	34.16391900	34.16035700	34.16035800	34.16035600
Q_{WG11}	[-25 30]	-2.0402	-2.0480	-2.0258	-2.0951	-2.0950	-2.0948
Q_{SG13}	[-20 25]	-12.3895	-12.3784	-12.3814	-12.4141	-12.4140	-12.4136
f_C(\$/h)		442.0876	442.2321	442.1089	435.9802	435.9756	435.9683
f_E(ton/h)		1.7748	1.7749	1.7747	1.0066	1.0066	1.0066
J_3		781.0738	781.0730	**781.0729**			
J_4					808.7237	808.7230	**808.7205**

Table 7. Results of the comparing to earlier studies in 30-bus system for cases 1-5

Methods	Case 1 f_C	Case 2 f_E	Case 3 f_{PL}	Case 4 J_1 $(f_C + \lambda f_{PL})$	Case 5 $J_2(f_C + \lambda f_{VD})$
HybridSFLA-SA[30]	801.79	0.2048			
ABC[7]	800.66	0.204826	3.1078		
BSA [46]	801.63		3.0844		
WTLBO [6]	800.57		3.109	1041.13	814.41
GPU-PSO [47]	800.53				
PPSOGSA [48]	800.528		3.1032		
ARCBBO [49]	800.5159	0.2048	3.1009		
SKH [50]	800.5141	0.2048	3.0987		
CGSCE [51]	800.5106	0.204823	3.1006		
MSA [18]	800.5099	0.20482	3.1005	1040.8075 (859.1915+40*4.5404)	814.15 (803.3125+100*0.10842)
COA [52]	800.5054		3.0952		
PSOGSA [53]	800.49859				814.06123 (804.43123+100*0.0963)
AGTLBO [54]	800.4811	0.2048	3.0906	1040.1928 (858.9928+40*4.5300)	813.2085 (803.7385 +100*0.0947)
HFAJAYA [55]	800.4800			1040.1885 (859.0165+40*4.5293)	813.1836 (803.7036 +100*0.0948)
ITWFO [56]	800.4787			1040.1889 (859.0009+40*4.5297)	813.2267 (803.8167+100*0.0941)
ISSA [57]	800.4752			1040.168 (859.5815+40*4.5139)	813.1898 (803.5848+100*0.0960)
EO [58]	800.4235				
IABC [59]	800.4215	0.1943*	3.0917		
ECHT-DE [14]	800.4131	0.20482	3,0844	1040.125 (859.1458+40*4.5245)	813.1742 (803.7198+100*0.09454)
IeJADE [60]	800.4115	0.2048	3.0840	1040.1127	813.1099
ACDE [61]	800.41132	0.204817	3.0840		
C2oDE-ECM-FR [62]	800.4112	0.204817	3.0839	1040.112	
IBSA [63]	800.3975	0.20482	3.0951		
DSA [16]	800.3887	0.205825	3.0945		
IMFO [15]	800.3848	0.2048	3.0905	1042.0255 (858.7455+40*4.582)	813.1115 (803,5715+100* 0,0954)
ESCA [64]	800.219[b]		3.021		814.1598 (804.9968+100*0.09163)
AMTPG-JAYA [65]	800.1946		3.0802		
AO-AOA [66]	800.0239[a1]	0.204820	3.01791[a1]		
AGOA	800.0212[b]	0.20484			
CS-GWO [67]	799.9978*		3.0861	1028.7028 (854.9948+40*4.3427)	813.777 (803.5477+100*0.1023)
MARO [68]	799.9548*	0.20479	3.0658	1037.719 (864.567+40*4.3288)	814.599 (803.056+100*0.110)
MGTO [8]	799.7888[c]	0.2047		1039.978 (855.7992+40*4.5353)	813.9268 (803.3351+100* 0.1059)
ST-IWO [69]	799.73[a2]	0.2047	2.981 [a3]	1037.248 (845.888+40*4.784)	
LTLBO [70]	799.4369[b]				813.4831 (803.7431+100* 0.0974)
IAOA [10]	799.151[b]	0.2046[b]	2.994[b]		813.89 (803.18+100*0.1071)
JS-MFO [71]	799.085[a4]	0.2047	2.881		813.484 (803.554 +100*0.0993)
TLBO [72]	799.0715[a3]				817.4771 (803.7871+100* 0.1369)
ICBO [17]	799.0353 [a5]				813.5378 (803.3978+100*0.1014)
ESHADE [12]	798.9152[b]	0.2047	2.823[b]	1022.2869 (851.4109+40* 4.2719)	813.1175 (803.6075+100*0.0951)
EBO	**800.3873**	0.2048	3.0779	1039.8552 (859.0432+40*4.5203)	**812.9074 (803.4714+100*0.0944)**
EBOCMAR	800.3878	0.2048	**3.0777**	1039.8632 (858.5683+40*4.5324)	812.9107 (803.4926+100*0.0942)
EBOCMARLS	800.3877	**0.20473**	3.0779	**1039.8364 (858.9914+40*0.9422)**	812.9317 (803.5331+100*0.094)

*Infeasible solution ([a1] The constraint on load bus voltage is violated because the voltage deviation was reported as 2.04713. On the other hand, given that the total active power generation is stated as 286.4988 MW, the active power loss amounts to 3.0988 MW. [a2, a3, a4, and a5]. The load bus voltage constraints have been violated due to reported voltage deviations of 1.4246, 1.65739, 1.8925, 1,6486 and 1.9652, respectively. [b] Load bus voltages and generator reactive power output values cannot be verified as they are not reported). [c]The control variables cannot be verified as they are not reported

For Cases 8, 9, and 10, which involve the addition of a hydro unit, the objective was to optimize fuel costs on the IEEE 30-bus system by integrating wind, solar, and hydro power sources. The typical characteristics of the wind, solar and tidal plants are detailed in Table 8. For this analysis, we assume that the output power of the hydro unit is influenced by the river flow velocity (Q_H), which adheres to a Gumbel distribution. The probability distribution of the river flow velocity can be summarized as follows:

$$f_Q(Q_H) = \frac{1}{\lambda} exp\left(\frac{Q_H-\gamma}{\lambda}\right) exp\left[-exp\left(\frac{Q_H-\gamma}{\lambda}\right)\right] \quad (40)$$

where γ shows the parameter of location, λ presents the parameter of scale, respectively. The hydro plant output generation is illustrated as in the following [34]:

$$P_H(Q_H) = \rho g Q_H H \eta. \quad (41)$$

where η shows the hydro turbine generation efficiency, ρ presents the density of water, g demonstrates acceleration resulting from the gravity, H gives the distance that exists between the highest and lowest levels of water, respectively. The mathematical values related with the hydro power generation parameters are represented by; $\rho = 1025\ kg/m^3$, $\eta = 0.85$, $H = 3.2\ m$, $g = 9.81\ m/s^2$.

Case 8 optimizes the production schedule for all thermal and renewable energy producers to minimize the total production cost given by equation (30.a). Detailed optimal results for the control and state variables obtained by EBO, EBO-CMAR, and EBO-CMAR-LS are presented in Table 8. EBO-CMAR-LS achieved the lowest production cost of 773.7706 $/hour and is highlighted in bold. In Figure 4.a, EBO-CMAR-LS, which incorporates the CMAR and LS components added to EBO, achieved the fastest convergence among the proposed algorithms. Considering the other two algorithms, their exploration and search capabilities were limited in the initial phase, whereas the algorithm with the LS component gained faster exploration and search capabilities.

Table 8. PDF parameters for stochastic models of wind, solar and hydro energy sources

Bus	P_R [MW]	v_{in}, v_r, v_{out} [m/s]	c, k	g, f	K_{RW}, K_{PW}	K_{RH}, K_{PH}	G [W/m^2]	μ, σ	e	γ, λ	K_{RS}, K_{PS}
8(wind)	45	3,16, 25	10,2	1.75	3,1.5	3, 1.5					
11(solar)	40						1000	5.2, 0.6	1.7		3, 1.65
13(wind+hydro)	30+10	3,16, 25	9, 2	1.6, 1.8	3, 1.5	3, 1.6				220, 24.5	

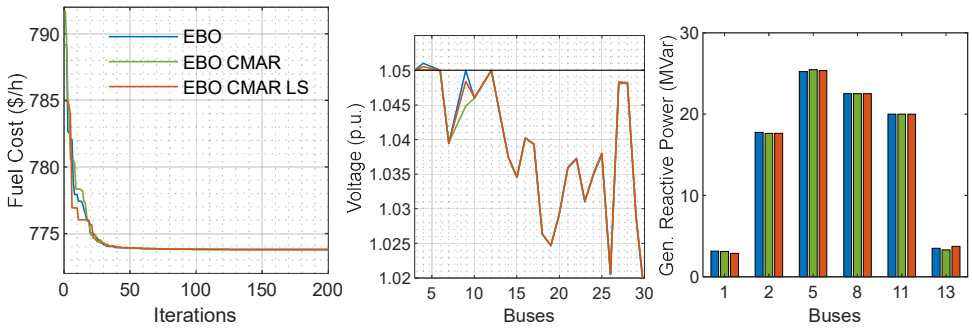

(a) (b) (c)

Figure 4. Fuel cost with renewable optimization for Case-8, (a) convergence curve (b) voltage profile (c) generator reactive power output.

The aim of case 9 is to minimize total fuel costs in a system integrating wind, solar, and hydro energy sources, taking into account the effect of the valve point in thermal generators. Table 9 shows the detailed results of the optimization process. The EBOCMARLS algorithm yielded the lowest value of $802.8085/hour. In case 10 the total cost was optimised through the use of the objective function given in (30.c). It is understood from the convergence curve and the results obtained in Fig. 5.a that the CMAR and LS parts do not make any extra contribution to the EBO algorithm.

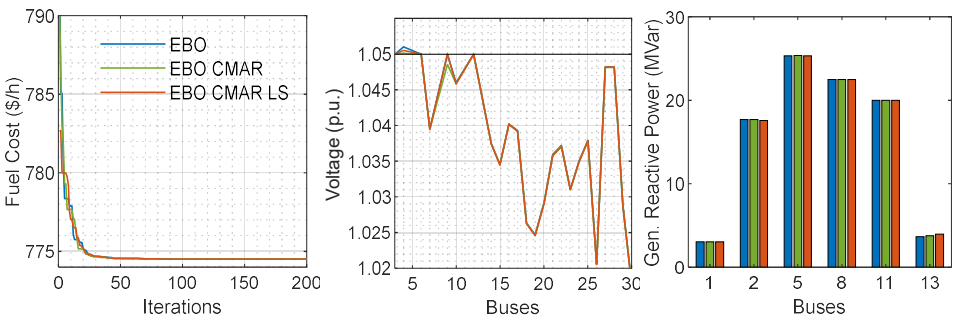

(a) (b) (c)

Figure 5. Fuel cost and fuel emission with renewable optimization for Case-10, (a) convergence curve (b) voltage profile (c) generator reactive power output.

Table 9. Simulation results of cases 8, 9, and 10 IEEE-30 bus modified test system with renewables

Items	Range	Case-8			Case-9			Case-10		
		EBO	EBOCMAR	EBOCMARLS	EBO	EBOCMAR	EBOCMARLS	EBO	EBOCMAR	EBOCMARLS
P_1	[50 200]	163.0920	163.0855	163.1028	140.0404	140.0125	140.0553	162.7573	162.7466	162.7747
P_2	[20 80]	45.2883	45.3091	45.2775	54.5360	54.5771	54.5407	45.4470	45.4497	45.4315
P_5	[15 50]	20.2924	20.2861	20.2958	19.9410	19.9407	19.9378	20.3486	20.3465	20.3457
P_{8wind}	[0 45]	28.1512	28.1396	28.1478	34.7427	34.7379	34.7237	28.2087	28.2176	28.2135
$P_{11solar}$	[0 30]	11.4452	11.4445	11.4449	13.5113	13.5113	13.5113	11.4452	11.4452	11.4451
$P_{13wind\&hydro}$	[0 40]	23.0972	23.1027	23.0975	27.5323	27.5262	27.5366	23.1414	23.1418	23.1378
V_1	[0.95 1.1]	1.0915	1.0915	1.0913	1.0861	1.0859	1.0862	1.0915	1.0915	1.0914
V_2	[0.95 1.1]	1.0532	1.0531	1.0530	1.0407	1.0505	1.0407	1.0531	1.0431	1.0431
V_5	[0.95 1.1]	1.0424	1.0426	1.0424	1.0410	1.0410	1.0411	1.0425	1.0425	1.0424
V_8	[0.95 1.1]	1.0580	1.0580	1.0580	1.0687	1.0587	1.0686	1.0580	1.0680	1.0680
V_{11}	[0.95 1.1]	1.0880	1.0830	1.0864	1.0876	1.0850	1.0862	1.0880	1.0866	1.0880
V_{13}	[0.95 1.1]	1.0542	1.0539	1.0545	1.0559	1.0553	1.0556	1.0544	1.0546	1.0548
$Q_{c\text{-}10}$	[0 30]	6.4795	7.4507	6.7109	6.1042	7.0302	6.3784	6.2714	6.3843	6.0767
$Q_{c\text{-}24}$	[0 30]	11.1167	11.2093	11.1851	11.1770	11.2560	11.2242	11.1812	11.1907	11.1497
T_{11}	[0.9 1.1]	1.0282	1.0438	1.0332	1.0285	1.0359	1.0329	1.0283	1.0323	1.0280
T_{12}	[0.9 1.1]	0.9396	0.9221	0.9332	0.9378	0.9321	0.9328	0.9387	0.9338	0.9389
T_{15}	[0.9 1.1]	0.9789	0.9786	0.9797	0.9824	0.9809	0.9818	0.9794	0.9796	0.9800
T_{16}	[0.9 1.1]	0.9767	0.9767	0.9765	0.9763	0.9770	0.9764	0.9767	0.9768	0.9766
Q_1	[-20 150]	3.1466	3.1128	2.8801	0.5877	0.6563	0.6873	3.0483	3.0293	3.0442
Q_2	[-20 60]	17.7383	17.6249	17.6167	15.4367	15.1517	15.4528	17.6799	17.6806	17.5850
Q_5	[-15 62.5]	25.2510	25.4763	25.3693	25.3804	25.5135	25.4465	25.3403	25.3530	25.3302
Q_8	[-18 22.5]	22.5000	22.4999	22.4999	22.5000	22.4999	22.5000	22.5000	22.4999	22.4998
Q_{11}	[-16 20]	19.9980	19.9958	19.9996	19.9999	19.9471	19.9999	20.0000	19.9893	19.9981
Q_{13}	[-16 20]	3.4843	3.2983	3.7388	4.9533	4.4414	4.7046	3.6522	3.7688	3.9741
f_E(t/h)		0.1901	0.1901	0.1901	0.1479	0.1478	0.1479	0.1893	0.1893	0.1894
f_{Pl}MW)		7.9662	7.9674	7.9663	7.0073	6.9056	6.9053	7.9482	7.9474	7.9482
f_{VD}(p.u)		0.9213	0.9174	0.9221	0.9170	0.9102	0.9156	0.9225	0.9198	0.9211
J_5		773.7707	773.7708	**773.7706**						
J_6					802.8086	802.8088	**802.8085**			
J_7								**774.4984**	**774.4984**	**774.4984**

Table 10. Comparison results with previous studies in the 30-bus system with integrated renewable energy sources for cases 6-10

Methods	Case 6	Case 7	Case 8	Case 9	Case 10
JS [73]	781.6387	810.1201			
DMOA [35]	780.989				
SHADE-SF [33]	782.503	810.346			
CMOPEO-EED [74]		809.518			
IEO [75]	782.0343				
ITWFO [56]	781.9943	810.1812			
EESWHO [76]	781.6322	808.462			
SAWGA [77]	782.0238	810.7448			
BMO [78]	781.6519	810.7982			
ICA [34]			773.9525	803.1826	777.8675
HS [34]			773.9589	803.1652	777.9504
BSA [34]			774.2297	803.3178	778.0258
SOS [34]			773.7797	802.6983	774.0652
EBO	781.0738	808.7237	773.7707	802.8086	**774.4984**
EBOCMAR	781.0730	808.7230	773.7708	802.8088	**774.4984**
EBOCMARLS	**781.0729**	**808.7205**	**773.7706**	**802.8085**	**774.4984**

V. VALIDITY AND QUALITY ANALYSIS OF THE SOLUTIONS

A. SECURITY CONSTRAINT VALIDATION FOR EBOwithCMAR AND ITS COMPONENTS

The operational and safety constraints must be strictly adhered to for the maintainability of a system. It is of the utmost importance to prevent violations of the limits inherent to the OPF problem. As previously stated in section 2.1, it is imperative that the reactive power of generators (Q_G), voltage limits (V_G) and line loads (S_{TL}) are maintained within the prescribed limits to ensure operational safety. Furthermore, it is essential to ensure that the voltage values at the load buses (V_L) remain within the specified minimum and maximum limits. In this study, the EBOwithCMAR approach is adapted to address the issue of undesirable solutions by introducing a penalty value into the objective function when solving the OPF problem with constraints.

Let $u = [P_G \quad V_G \quad Q_C \quad T]$ denote any solution vector and x denote the vector of constraint parameters, represented by $x = [P_{Gslack} \quad Y]$, where $Y = [V_L \; Q_G \; S_{TL}]$. Subsequently, the objective function value, $f(x)$, is updated through a series of sequential operations, as outlined in Eqs. (42)-(45), in order to penalise

any instances of non-compliance with the specified boundaries. In the event of a slack variable exceeding the prescribed limits, a penalty of 1000 is applied, as illustrated in Eq. (43).

$$[P_{Glsack}, Y] = PowerFlow(x)\ . \qquad (42)$$

$$P_{Glsack} = 1000.P_{Glsack}.(P_{Glsack} > Ub_{Glsack} || P_{Glsack} < Lb_{Glsack}) \qquad (43)$$

$$Penalty(Y) = w.\sum_{i=1}^{n}[abs(Ub_i - Y_i).(Y_i > Ub_i) + abs(Lb_i - Y_i).(Y_i < Lb_i)]\ , \qquad (44)$$

where $PowerFlow(x)$ is defined according to the definition provided by [79], Ub_{Glsack} and Lb_{Glsack} are upper and lower bounds of the slack variable respectively, Ub_i and Lb_i are upper and lower bounds of the *i.* constraint parameters respectively, *w* is the penalty coefficient and empirically found for each multi-objective function definition. Then, the objective function value,$f(x)$, used in the algorithm is updated by Eq. (45) where the objective function uses the slack variable as defined in Eq. (43) (if applicable) and adds a further penalty to any violating bounds.

$$f(x) = f(x) + Penalty(Y). \qquad (45)$$

As illustrated in Tables 3 and 4, the optimal solution sets obtained by the proposed algorithms with the applied penalty technique method remain within the prescribed safety and operational limits. Figs. 1(b), 2(b), 3(b), 4(b) and 5(b), along with Figs. 1(c), 2(c), 3(c), 4(c) and 5(c) illustrate two critical parameters, namely load bus voltage and generator reactive power for IEEE 30 bus system without renewable energy sources. The plots for each case are presented to demonstrate that the load and generator buses do not exceed the upper and lower limits. The data presented in Figs. 1(b), 2(b), 3(b), 4(b) and 5(b) demonstrate that the load bus voltage values (1.05 p.u) for Case 1, Case 2, Case 3, Case 4 and Case 5 are below the black line, which has been drawn from the upper limit value. A careful examination of Figs. 1(b), 2(b), 3(b) and 4(b) reveal that the bus voltages frequently approach their limits due to constraints in the load bus voltages, particularly in case 1 and case 4. In contrast, there is a direct correlation between reactive power and voltage. Although buses 10 and 12 have reactive power support, the EBOCMAR algorithm and its components made an extraordinary effort in the search process of solution points. They managed to keep the bus voltages below 1.05 p.u with less reactive power support. Additionally, Figs. 1(c), 2(c), 3(c), 4(c), and 5(c) show the reactive power outputs generated in response to the specified limits. It is evident from these figures that the constraints are not violated for any of the algorithms under consideration. This demonstrates the high efficacy in attaining optimal solutions. In cases 1, 2, and 3, where the single objective optimal power flow problem is considered, it can be observed that the CMAR component enhances the exploration of the search space. The impact of the CMAR component on generator reactive power output values is evident in Figs. 2 and 3.Table 6 indicates the optimal results of the control variables for resolving two optimal power flow problems with single and multiple objectives in the IEEE 30 bus test system, including renewable energy sources. The bus voltages versus the considered limits for all the implemented algorithms are illustrated in Figs. 4(b) and 5(b). Also, Figs. 4(c) and 5(c) demonstrate a comparison of the generated reactive power outputs against the specified limits. It is evident from these figures that no violations have occurred.

B. STATISTICAL COMPARISON AMONG EBO, EBOCMAR AND EBO CMAR LS(EBOwithCMAR)

The performance of the algorithms is presented in the spider graph in Fig. 6, without violating all system constraints for each performed study case (i.e. from case 1 to case 10). CMAR enhances the search direction and diversity of solutions by employing the covariance matrix to facilitate a more intelligent optimization process, whereas LS augments the precision and accuracy of the final solutions by implementing a more concentrated search. Once CMAR has identified a promising region, the solution can be fully optimized. Therefore, the EBO with CMAR and LS approach has been optimized to its fullest extent by minimizing the objective functions in cases 2, 4, 6, 7, 8 and 9. In cases 3 and 5, where the objective functions are relatively simple, such as the minimization of active power loss and voltage deviation, the performance of EBOwithCMAR is the poorest. Nevertheless, EBOwithCMAR demonstrates superior performance compared to EBO and EBOCMAR in all more complex and uncertain scenarios involving renewable energy sources.

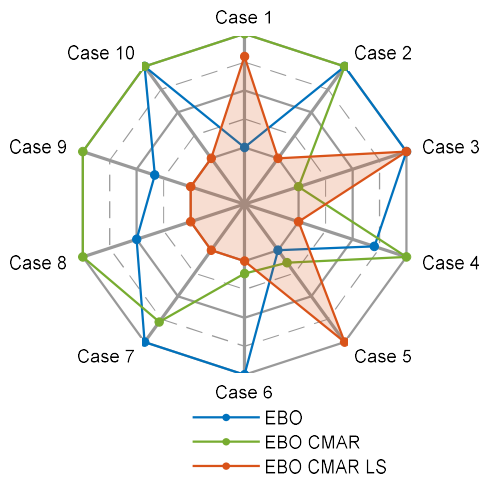

Figure 6. Spider chart with ten cases.

C. COMPARATIVE ANALYSIS

Compared with the literature results presented in Table 7, except for the infeasible solutions, for Case 1, the proposed EBO, EOBCMAR and EBOCMARLS algorithms have left many studies behind. Except for AMTPG-JAYA [65], which gave better results than the proposed method, which resulted in 800.1946 $/h, better results were obtained than IMFO [15], DSA [16], and IBSA [63] algorithms reached the best values of 800.3848, 800.3887, and 800.3975 $/h, respectively. Also, for Case 2, it can be seen that the 0.2047 ton/h results obtained by ESHADE [12], ST-IWO [69] and MGTO [8] are close to the 0.2047 ton/h result obtained by EBOCMARLS. However, this result is lower than the presented studies such as MARO [68] 0.20479 ton/h, IMFO [15] 0.2048 ton/h, DSA [16] 0.205825 ton/h, and IBSA [63] 0.20482 ton/h. In addition, when the results obtained in the literature are compared for Case 3, it is observed that, except for the value of 3.0658 obtained with MARO [68], a better result is obtained from the studies that are closest to the optimal result, namely IMFO [15] with 3.0905, DSA [16] with 3.0945, IBSA [63] with 3.0951, C2oDE-ECM-FR [62] with 3.0839 and ACDE [61] with 3.0840. For Case 4, the closest value to the result found among the feasible solutions, 1039.8364, is obtained with IMFO [15] with 1042.0255. Apart from this, the results of 1040.112, 1040.1127, 1040.125 and 1040.168 that are obtained by

C2oDE-ECM-FR [62], IєJADE [60], ECHT-DE [14] and ISSA [57] methods are further away from the result obtained with EBOCMARLS. Also, for Case 5, in the studies given by literature, EBO left behind IMFO [15], which presented a result of 813.1115, DSA [16], which obtained 813.1115, IєJADE [60], which reached the optimal value of 813.1099, ECHT-DE [14], which reached a result of 813.1742, and many other studies with 812.9074. As the results presented by studies in the literature examined for Case 6, the EBOCMARLS algorithm converges to a lower value and was able to outperform 781.6387, 780.989, 782.503, 782.0343, 781.9943, 781.6322, 782.0238 and 781.6519, respectively; which are obtained by JS [73], DMOA [35], SHADE-SF [33], CMOPEO-EED [74], IEO [75] ITWFO [56], EESWHO [76], SAWGA [77] and BMO [78] methods. When Table 10 is examined for Case 7, the EBOCMARLS algorithm outperforms the methods JS [73], DMOA [35], SHADE-SF [33], CMOPEO-EED [74], IEO [75], ITWFO [56], SAWGA [77] and BMO [78], which converged to the values of 810.120, 810.346, 809.518, 810.1812, 810.7448, 810.7982, respectively. The contribution of the LS component in cases 8, 9, and 10, where hydro energy sources are integrated, has provided a competitive improvement compared to the EBO and EBOCMAR algorithms. In particular, in Case 8, EBOCMARLS achieved lower cost values than the ICA [34], and SOS [34] algorithms, with its outstanding performance. In cases 9 and 10, the proposed model demonstrated superior performance in comparison to the ICA [34] and HS [34] algorithms.

A key limitation of this study is its exclusive focus on the IEEE 30-bus test system. Although this benchmark is standard in the literature and supports comparison with prior work, validation on larger or more complex systems, such as the IEEE 57-bus, IEEE 118-bus, or real-world networks, is necessary to confirm the broader applicability of the results. Moreover, the small performance differences reported here may partly reflect the relatively stable optimization characteristics of the selected benchmark.

VI. CONCLUSION

In this paper, we have demonstrated that EBOwithCMAR and its components can solve single and multi-objective OPF problems while adhering to all constraints. The optimization of power system, which is becoming increasingly complex with integrating renewable energy sources, has been extensively performed. We present the optimization results clearly and in detail, supported by tables and graphs showing that the constraints are not violated. Our findings show that SOOPF and weighted method MOOPF for IEEE 30 bus test system can be successfully managed by EBO, EBOCMAR, and EBOCMARLS algorithms. We compare our methodology with well-established algorithms in the literature and identify promising results that preserve all system constraints. While the proposed EBOwithCMAR and its component algorithms achieve competitive results that rank among the best reported in the literature, we acknowledge that the improvements over the State-of-the-Art are marginal (typically 0.5–1.0% across benchmark cases). This finding is itself a valid scientific contribution, as it demonstrates that all mature metaheuristic algorithms exhibit similar convergence behavior on the IEEE 30-bus benchmark problem.

References

[1] F. Daqaq, M. Ouassaid, R. Ellaia, "A new meta-heuristic programming for multi-objective optimal power flow," *Electrical Engineering*, vol. 103, pp. 1217–1237, 2021. https://doi.org/10.1007/s00202-020-01173-6.

[2] J. Zhang, Q. Tang, P. Li, D. Deng, Y. Chen, "A modified MOEA/D approach to the solution of multi-objective optimal power flow problem," *Applied Soft Computing Journal*, vol. 47, pp. 494-514, 2016. https://doi.org/10.1016/j.asoc.2016.06.022.

[3] T.H.B. Huy, D. Kim, D.N. Vo, "Multiobjective optimal power flow using multiobjective search group algorithm," *IEEE Access*, vol. 10, pp. 77837-77856,, 2022. https://doi.org/10.1109/ACCESS.2022.3193371.

[4] U. Nangia, N.K. Jain, C.L. Wadhwa, "Optimal weight assessment based on a range of objectives in a multiobjective optimal load flow study," *IEE Proceedings: Generation, Transmission and Distribution*, vol. 145, 1998. https://doi.org/10.1049/ip-gtd:19981655.

[5] R.S. Salgado, E.L. Rangel, "Optimal power flow solutions through multi-objective programming," *Energy*, vol. 42, issue 1, pp. 35-45, 2012. https://doi.org/10.1016/j.energy.2011.11.028.

[6] S. Ermiş, "Multi-objective optimal power flow using a modified weighted teaching-learning based optimization algorithm," *Electric Power Components and Systems*, vol. 51, issue 20, pp. 2536-2556, 2023. https://doi.org/10.1080/15325008.2023.2239237.

[7] M. Rezaei Adaryani, A. Karami, "Artificial bee colony algorithm for solving multi-objective optimal power flow problem," *International Journal of Electrical Power and Energy Systems*, vol. 53, pp. 219-230, 2013. https://doi.org/10.1016/j.ijepes.2013.04.021.

[8] R. Jamal, J. Zhang, B. Men, N.H. Khan, M. Ebeed, T. Jamal, E.A. Mohamed, "Chaotic-quasi-oppositional-phasor based multi populations gorilla troop optimizer for optimal power flow solution", *Energy*, vol. 301, 131684, 2024. https://doi.org/10.1016/J.ENERGY.2024.131684.

[9] T.M. Dao, T.H.B. Huy, D.P.N. Do, D. Ngoc Vo, "A chaotic equilibrium optimization for temperature-dependent optimal power flow," *Smart Science*, vol. 11, issue 2, pp. 380-394, 2023. https://doi.org/10.1080/23080477.2023.2171696.

[10] O. Akdag, "A improved archimedes optimization algorithm for multi/single-objective optimal power flow," *Electric Power Systems Research*, vol. 206, 107796, 2022. https://doi.org/10.1016/j.epsr.2022.107796.

[11] A.E. Chaib, H.R.E.H. Bouchekara, R. Mehasni, M.A. Abido, "Optimal power flow with emission and non-smooth cost functions using backtracking search optimization algorithm," *International Journal of Electrical Power and Energy Systems*, vol. 81, pp. 64-77, 2016. https://doi.org/10.1016/j.ijepes.2016.02.004.

[12] M. Premkumar, C. Kumar, T.D. Raj, S.D.T.S. Jebaseelan, P. Jangir, H.H. Alhelou, "A reliable optimization framework using ensembled successive history adaptive differential evolutionary algorithm for optimal power flow problems," *IET Generation, Transmission & Distribution*, vol. 17, 1333–1357, 2023. https://doi.org/10.1049/gtd2.12738.

[13] R. Keswani, H.K. Verma, S.K. Sharma, "Multi-objective optimal power flow employing a hybrid sine cosine – Grey Wolf Optimizer," *Iranian Journal of Science and Technology – Transactions of Electrical Engineering*, vol. 47, pp. 1365–1388, 2023. https://doi.org/10.1007/s40998-023-00631-8.

[14] P.P. Biswas, P.N. Suganthan, R. Mallipeddi, G.A.J. Amaratunga, "Optimal power flow solutions using differential evolution algorithm integrated with effective constraint handling techniques," *Eng Appl Artif Intell*, vol. 68, pp. 81-100, 2018. https://doi.org/10.1016/j.engappai.2017.10.019.

[15] M.A. Taher, S. Kamel, F. Jurado, M. Ebeed, "An improved moth-flame optimization algorithm for solving optimal power flow problem," *International Transactions on Electrical Energy Systems*, vol. 29, e2743, 2019. https://doi.org/10.1002/etep.2743.

[16] K. Abaci, V. Yamacli, "Differential search algorithm for solving multi-objective optimal power flow problem," *International Journal of Electrical Power and Energy Systems*, vol. 79, pp. 1-10, 2016. https://doi.org/10.1016/j.ijepes.2015.12.021.

[17] H.R.E.H. Bouchekara, A.E. Chaib, M.A. Abido, R.A. El-Sehiemy, "Optimal power flow using an improved colliding bodies optimization algorithm," *Applied Soft Computing Journal*, vol. 42, pp. 119-131, 2016. https://doi.org/10.1016/j.asoc.2016.01.041.

[18] A.A.A. Mohamed, Y.S. Mohamed, A.A.M. El-Gaafary, A.M. Hemeida, "Optimal power flow using moth swarm algorithm," *Electric Power Systems Research*, vol. 142, pp. 190-206, 2017. https://doi.org/10.1016/j.epsr.2016.09.025.

[19] T. Niknam, M. Rasoul Narimani, M. Jabbari, A.R. Malekpour, "A modified shuffle frog leaping algorithm for multi-objective optimal power flow," *Energy*, vol. 36, issue 11, pp. 6420-6432, 2011. https://doi.org/10.1016/j.energy.2011.09.027.

[20] H. Pulluri, R. Naresh, V. Sharma, "An enhanced self-adaptive differential evolution based solution methodology for multiobjective optimal power

flow," *Applied Soft Computing Journal*, vol. 54, pp. 229-245, 2017. https://doi.org/10.1016/j.asoc.2017.01.030.

[21] B. Mandal, P. Kumar Roy, "Multi-objective optimal power flow using quasi-oppositional teaching learning based optimization," *Applied Soft Computing Journal*, vol. 21, pp. 590-606, 2014. https://doi.org/10.1016/j.asoc.2014.04.010.

[22] A. Shabanpour-Haghighi, A.R. Seifi, T. Niknam, "A modified teaching-learning based optimization for multi-objective optimal power flow problem," *Energy Convers Manag*, vol. 77, pp. 597-607, 2014. https://doi.org/10.1016/j.enconman.2013.09.028.

[23] M. Ahmadipour, Z. Ali, V.K. Ramachandaramurthy, H.M. Ridha, "A memory-guided Jaya algorithm to solve multi-objective optimal power flow integrating renewable energy sources," *Appl Soft Comput*, vol. 164, 111924, 2024. https://doi.org/10.1016/J.ASOC.2024.111924.

[24] E.E. Elattar, S.K. ElSayed, "Modified JAYA algorithm for optimal power flow incorporating renewable energy sources considering the cost, emission, power loss and voltage profile improvement," *Energy*, vol. 178, pp. 598-609, 2019. https://doi.org/10.1016/j.energy.2019.04.159.

[25] S. Li, W. Gong, L. Wang, Q. Gu, "Multi-objective optimal power flow with stochastic wind and solar power," *Appl Soft Comput*, vol. 114, 108045, 2022. https://doi.org/10.1016/j.asoc.2021.108045.

[26] A. Man-Im, W. Ongsakul, J.G. Singh, M.N. Madhu, "Multi-objective optimal power flow considering wind power cost functions using enhanced PSO with chaotic mutation and stochastic weights," *Electrical Engineering*, vol. 101, pp. 699–718, 2019. https://doi.org/10.1007/s00202-019-00815-8.

[27] S.B. Pandya, H.R. Jariwala, "Renewable energy resources integrated multi-objective optimal power flow using non-dominated sort grey wolf optimizer," *Journal of Green Engineering*, vol. 10, 2020.

[28] J. Zhu, Y. Zhou, Y. Wei, Q. Luo, H. Huang, "Optimal stochastic power flow using enhanced multi-objective mayfly algorithm," *Heliyon*, vol. 10, issue 5, e26427, 2024. https://doi.org/10.1016/j.heliyon.2024.e26427.

[29] A. Kumar, R.K. Misra, D. Singh, "Improving the local search capability of effective butterfly optimizer using covariance matrix adapted retreat phase," *Proceedings of the 2017 IEEE Congress on Evolutionary Computation, CEC'2017*, Donostia, Spain, 2017, pp. 1835-1842. https://doi.org/10.1109/CEC.2017.7969524.

[30] T. Niknam, M.R. Narimani, R. Azizipanah-Abarghooee, "A new hybrid algorithm for optimal power flow considering prohibited zones and valve point effect," *Energy Convers Manag*, vol. 58, pp. 197-206, 2012. https://doi.org/10.1016/j.enconman.2012.01.017.

[31] L. Shi, C. Wang, L. Yao, Y. Ni, M. Bazargan, "Optimal power flow solution incorporating wind power," *IEEE Syst J*, vol. 6, pp. 233–241, 2012. https://doi.org/10.1109/JSYST.2011.2162896.

[32] T.P. Chang, "Investigation on frequency distribution of global radiation using different probability density functions," *International Journal of Applied Science and Engineering*, vol. 8, 2010.

[33] P.P. Biswas, P.N. Suganthan, G.A.J. Amaratunga, "Optimal power flow solutions incorporating stochastic wind and solar power," *Energy Convers Manag*, vol. 148, pp. 1194-1207, 2017. https://doi.org/10.1016/j.enconman.2017.06.071.

[34] S. Duman, J. Li, L. Wu, "AC optimal power flow with thermal–wind–solar–tidal systems using the symbiotic organisms search algorithm," *IET Renewable Power Generation*, vol. 15, pp. 278-296, 2021. https://doi.org/10.1049/rpg2.12023.

[35] S. Mouassa, A. Alateeq, A. Alassaf, R. Bayindir, I. Alsaleh, F. Jurado, "Optimal power flow analysis with renewable energy resource uncertainty using dwarf mongoose optimizer: Case of ADRAR isolated electrical network," *IEEE Access*, vol. 12, pp. 10202-10218, 2024. https://doi.org/10.1109/ACCESS.2024.3351721.

[36] A. Kumar, R.K. Misra, D. Singh, "Butterfly optimizer," *Proceedings of the 2015 IEEE Workshop on Computational Intelligence: Theories, Applications and Future Directions (WCI)*, 2015, pp. 1–6. https://doi.org/10.1109/WCI.2015.7495523.

[37] D. Zaharie, "A comparative analysis of crossover variants in differential evolution, *Proceedings of the IMCSIT*, 2007.

[38] R. Tanabe, A.S. Fukunaga, "Improving the search performance of SHADE using linear population size reduction," *Proceedings of the 2014 IEEE Congress on Evolutionary Computation, CEC'2014*, Beijing, China, 2014, pp. 1658-1665. https://doi.org/10.1109/CEC.2014.6900380.

[39] R. Tanabe, A. Fukunaga, "Success-history based parameter adaptation for differential evolution," *Proceedings of the 2013 IEEE Congress on Evolutionary Computation, CEC'2013*, Cancun, Mexico, 2013, pp. 71-78. https://doi.org/10.1109/CEC.2013.6557555.

[40] N. Hansen, S.D. Müller, P. Koumoutsakos, "Reducing the time complexity of the derandomized evolution strategy with covariance matrix adaptation (CMA-ES)," *Evol Comput*, vol. 11, issue 1, pp. 1-18, 2003. https://doi.org/10.1162/106365603321828970.

[41] N. Hansen, "The CMA evolution strategy: A tutorial," ArXiv Preprint ArXiv:1604.00772, 2016.

[42] S. Elsayed, N. Hamza, R. Sarker, "Testing united multi-operator evolutionary algorithms-II on single objective optimization problems," *Proceedings of the 2016 IEEE Congress on Evolutionary Computation, CEC'2016*, 2016, pp. 2966-2973. https://doi.org/10.1109/CEC.2016.7744164.

[43] O. Alsac, B. Stott, "Optimal load flow with steady-state security," *IEEE Transactions on Power Apparatus and Systems*, vol. PAS-93, no. 3, pp. 745-751, 1974. https://doi.org/10.1109/TPAS.1974.293972.

[44] R.D. Zimmerman, C.E. Murillo-Sánchez, MATPOWER, 2020. https://doi.org/10.5281/zenodo.4074135.

[45] M. Shahidehpour, Y. Wang, "Appendix C: IEEE30 Bus System Data," *Communication and Control in Electric Power Systems: Applications of Parallel and Distributed Processing*, 2003, pp. 493–495. https://doi.org/10.1002/0471462926.app3.

[46] U. Kılıç, "Backtracking search algorithm-based optimal power flow with valve point effect and prohibited zones," *Electrical Engineering*, vol. 97, pp. 101–110, 2015. https://doi.org/10.1007/s00202-014-0315-0.

[47] V. Roberge, M. Tarbouchi, F. Okou, "Optimal power flow based on parallel metaheuristics for graphics processing units," *Electric Power Systems Research*, vol. 140, pp. 344-353, 2016. https://doi.org/10.1016/j.epsr.2016.06.006.

[48] Z. Ullah, S. Wang, J. Radosavljevic, J. Lai, "A Solution to the optimal power flow problem considering WT and PV Generation," *IEEE Access*, vol. 7, pp. 46763-46772, 2019. https://doi.org/10.1109/ACCESS.2019.2909561.

[49] A. Ramesh Kumar, L. Premalatha, "Optimal power flow for a deregulated power system using adaptive real coded biogeography-based optimization," *International Journal of Electrical Power and Energy Systems*, vol. 73, pp. 393-399, 2015. https://doi.org/10.1016/j.ijepes.2015.05.011.

[50] H. Pulluri, R. Naresh, V. Sharma, "A solution network based on stud krill herd algorithm for optimal power flow problems," *Soft Comput*, vol. 22, pp. 159–176, 2018. https://doi.org/10.1007/s00500-016-2319-3.

[51] H. Su, Q. Niu, Z. Yang, "Optimal power flow using improved cross-entropy method," *Energies*, vol. 16, issue 14, 5466, 2023. https://doi.org/10.3390/en16145466.

[52] J.H. Zhu, J.S. Wang, X.Y. Zhang, H.M. Song, Z.H. Zhang, "Mathematical distribution coyote optimization algorithm with crossover operator to solve optimal power flow problem of power system," *Alexandria Engineering Journal*, vol. 69, pp. 585-612, 2023. https://doi.org/10.1016/j.aej.2023.02.023.

[53] J. Radosavljević, D. Klimenta, M. Jevtić, N. Arsić, "Optimal power flow using a hybrid optimization algorithm of particle swarm optimization and gravitational search algorithm," *Electric Power Components and Systems*, vol. 43, issue 17, pp. 1958-1970, 2015. https://doi.org/10.1080/15325008.2015.1061620.

[54] A. Alanazi, M. Alanazi, Z.A. Memon, A. Mosavi, "Determining optimal power flow solutions using new adaptive Gaussian TLBO method," *Applied Sciences*, vol. 12, issue 16, 7959, 2022. https://doi.org/10.3390/app12167959.

[55] A.S. Alghamdi, "A hybrid firefly–JAYA algorithm for the optimal power flow problem considering wind and solar power generations," *Applied Sciences*, vol. 12, issue 14, 7193, 2022. https://doi.org/10.3390/app12147193.

[56] A.S. Alghamdi, "Optimal power flow of hybrid wind/solar/thermal energy integrated power systems considering costs and emissions via a novel and efficient search optimization algorithm," *Applied Sciences*, vol. 13, issue 8, 4760, 2023. https://doi.org/10.3390/app13084760.

[57] S. Abd El-Sattar, S. Kamel, M. Ebeed, F. Jurado, "An improved version of salp swarm algorithm for solving optimal power flow problem," *Soft Comput*, vol. 25, pp. 4027–4052, 2021. https://doi.org/10.1007/s00500-020-05431-4.

[58] M. Amroune, "Wind integrated optimal power flow considering power losses, voltage deviation, and emission using equilibrium optimization algorithm," *Energy Ecol Environ*, vol. 7, pp. 369–392, 2022. https://doi.org/10.1007/s40974-022-00249-2.

[59] X. He, W. Wang, J. Jiang, L. Xu, "An improved artificial bee colony algorithm and its application to multi-objective optimal power flow," *Energies*, vol. 8, issue 4, 2412, 2015 https://doi.org/10.3390/en8042412.

[60] W. Yi, Z. Lin, Y. Lin, S. Xiong, Z. Yu, Y. Chen, "Solving optimal power flow problem via improved constrained adaptive differential evolution," *Mathematics*, vol. 11, issue 5, 1250, 2023. https://doi.org/10.3390/math11051250.

[61] S. Li, W. Gong, C. Hu, X. Yan, L. Wang, Q. Gu, "Adaptive constraint differential evolution for optimal power flow," *Energy*, vol. 235, 121362, 2021. https://doi.org/10.1016/j.energy.2021.121362.

[62] A. Ali, A. Hassan, M.U. Keerio, N.H. Mugheri, G. Abbas, M. Hatatah, E. Touti, A. Yousef, "A novel solution to optimal power flow problems

using composite differential evolution integrating effective constrained handling techniques," *Sci Rep*, vol. 14, 6187, 2024. https://doi.org/10.1038/s41598-024-56590-5.

[63] M. Ahmad, N. Javaid, I.A. Niaz, I. Ahmed, M.A. Hashmi, "An orthogonal learning bird swarm algorithm for optimal power flow problems, *IEEE Access*, vol. 11, pp. 23659-23680, 2023. https://doi.org/10.1109/ACCESS.2023.3253796.

[64] A. Messaoudi, M. Belkacemi, "Optimal power flow solution using efficient sine cosine optimization algorithm," International Journal of Intelligent Systems and Applications, vol. 15, pp. 34-43, 2020. https://doi.org/10.5815/ijisa.2020.02.04.

[65] W. Warid, "Optimal power flow using the AMTPG-Jaya algorithm," *Applied Soft Computing Journal*, vol. 91, 106252, 2020. https://doi.org/10.1016/j.asoc.2020.106252.

[66] M. Ahmadipour, M. Murtadha Othman, R. Bo, M. Sadegh Javadi, H. Mohammed Ridha, M. Alrifaey, "Optimal power flow using a hybridization algorithm of arithmetic optimization and aquila optimizer," *Expert Syst Appl*, vol. 235, 121212, 2024. https://doi.org/https://doi.org/10.1016/j.eswa.2023.121212.

[67] A. Meng, C. Zeng, P. Wang, D. Chen, T. Zhou, X. Zheng, H. Yin, "A high-performance crisscross search based grey wolf optimizer for solving optimal power flow problem," *Energy*, vol. 225, 120211, 2021. https://doi.org/10.1016/j.energy.2021.120211.

[68] N.H. Khan, Y. Wang, R. Jamal, S. Iqbal, M. Ebeed, M.M. Khan, Y.Y. Ghadi, Z.M.S. Elbarbary, "Solving optimal power flow frameworks using modified artificial rabbit optimizer," *Energy Reports*, vol. 12, pp. 3883–3903, 2024. https://doi.org/10.1016/J.EGYR.2024.09.020.

[69] M. Kaur, N. Narang, "Optimal power flow solution using space transformational invasive weed optimization algorithm," *Iranian Journal of Science and Technology – Transactions of Electrical Engineering*, vol. 47, pp. 939–965, 2023. https://doi.org/10.1007/s40998-023-00592-y.

[70] M. Ghasemi, S. Ghavidel, M. Gitizadeh, E. Akbari, "An improved teaching-learning-based optimization algorithm using Lévy mutation strategy for non-smooth optimal power flow," *International Journal of Electrical Power and Energy Systems*, vol. 65, pp. 375-384, 2015. https://doi.org/10.1016/j.ijepes.2014.10.027.

[71] C. Mayouf, A. Salhi, F. Haidara, F.Z. Aroua, R.A. El-Sehiemy, D. Naimi, C. Aya, C.S.E. Kane, "Solving optimal power flow using new efficient hybrid jellyfish search and moth flame optimization algorithms," *Algorithms*, vol. 17, issue 10, 438, 2024. https://doi.org/10.3390/a17100438.

[72] H.R.E.H. Bouchekara, M.A. Abido, M. Boucherma, "Optimal power flow using teaching-learning-based optimization technique," *Electric Power Systems Research*, vol. 114, pp. 49-59, 2014. https://doi.org/10.1016/j.epsr.2014.03.032.

[73] M. Farhat, S. Kamel, A.M. Atallah, B. Khan, "Optimal power flow solution based on jellyfish search optimization considering uncertainty of renewable energy sources," *IEEE Access*, vol. 9, pp. 100911-100933, 2021. https://doi.org/10.1109/ACCESS.2021.3097006.

[74] M.R. Chen, G.Q. Zeng, K. Di Lu, Constrained multi-objective population extremal optimization based economic-emission dispatch incorporating renewable energy resources," *Renew Energy*, vol. 143, 277-294, 2019. https://doi.org/10.1016/j.renene.2019.05.024.

[75] N.A. Nguyen, D.N. Vo, T.T. Nguyen, T.L. Duong, "An improved equilibrium optimizer algorithm for solving optimal power flow problem with penetration of wind and solar energy," *International Transactions on Electrical Energy Systems*, vol. 2022, 7827164, 21 pages, 2022. https://doi.org/10.1155/2022/7827164.

[76] M.H. Hassan, S. Kamel, A.G. Hussien, "Optimal power flow analysis considering renewable energy resources uncertainty based on an improved wild horse optimizer," *IET Generation, Transmission and Distribution*, vol. 17, pp. 3582–3606, 2023. https://doi.org/10.1049/gtd2.12900.

[77] P. Trojovský, E. Trojovská, E. Akbari, "Economical-environmental-technical optimal power flow solutions using a novel self-adaptive wild geese algorithm with stochastic wind and solar power," *Sci Rep*, vol. 14, 4135, 2024. https://doi.org/10.1038/s41598-024-54510-1.

[78] M.H. Sulaiman, Z. Mustaffa, "Optimal power flow incorporating stochastic wind and solar generation by metaheuristic optimizers," *Microsystem Technologies*, vol. 27, pp. 3263–3277, 2021. https://doi.org/10.1007/s00542-020-05046-7.

[79] H. Saadat, *Power System Analysis*, Third Edition, Systems, Controls, Embedded Systems, Energy, and Machines, vol. 3, 2011.

***IBRAHIM CAGRI BARUTCU** received the B.Sc. degree from the Department of Electrical and Electronics Engineering, Eskisehir Osmangazi University, Eskişehir, Türkiye, in 2011, and the M.Sc. and Ph.D. degrees in electrical and electronics engineering from Ege University, İzmir, Türkiye, in 2014 and 2020, respectively. He is currently an Assistant Professor with the Department of Electricity and Energy, Hakkari University. His research interests include harmonic power quality in active distribution networks, renewable energy resources, distributed generation planning, and optimization methods.*

***VOLKAN YAMAÇLI** received the M.Sc. and Ph.D. degrees in electrical-elect ronics engineering from the Institute of Applied Sciences, Mersin University, Türkiye, in 2014 and 2021, respectively. He is currently an Assistant Professor with the Department of Computer Engineering, Mersin University. He is the author or co-author of more than 40 publications in journals and conferences. His current research interests include hybrid power and energy systems, deep learning, and artificial intelligence solutions.*

***HAKAN IŞIKER,** received the Ph.D. degree in electrical and electronics engineering from Mersin University, Mersin, Türkiye, in 2020. He is currently an Assistant Professor with the Electrical and Electronics Engineering Department, Mersin University. He is the author or co-author of more than 20 publications in journals and conferences. His research interests include passive radar imaging systems, synthetic aperture radar (SAR) focusing algorithms, image processing, target detection techniques, optimization, and artificial intelligence algorithms.*

***KADİR ABACI** received the B.Sc. degree in electrical and electronics engineering from Istanbul Technical University, in 1993, and the M.Sc. and Ph.D. degrees in electrical and electronics engineering from Sakarya University, in 2003 and 2007, respectively. He is a Professor of Electrical and Electronics Engineering at Mersin University. He has done academic work in the Mersin University. The author has more than 50 publications, including original publications and conferences. His research, mostly in the field of voltage stability of the power systems, power system optimization, and its control applications.*

***ELİF ECE ELMAS** received her Ph.D. degree in Electrical and Electronics Engineering from Gazi University, Türkiye. She also obtained her M.Sc. degree in Electrical and Electronics Engineering from the same university in 2019. She is currently an Assistant Professor at the National Defence University, Türkiye. Her research interests include unmanned aerial vehicles, sensor fusion, navigation systems, electronic warfare, and optimization techniques.*